# A high-cycle accumulation model for sand

A. Niemunis,* T. Wichtmann,† Th. Triantafyllidis‡

## Abstract

A high-cycle explicit model for the accumulation of strain in sand due to small cyclic loading is presented. The dependence of the accumulation rate on stress, void ratio, cyclic history and the type of loading is discussed. In particular, the ovality and the polarization of the strain path during a cycle are considered. Attention is given to the theoretical aspects of the constitutive description of the cumulative settlement and to the FE-implementation. The essential experimental results are also presented. Finally, an example of an FE-analysis of a strip foundation under cyclic vertical loading is given.

**Keywords:** *cyclic loading, sand, high-cycle, accumulation, settlement, amplitude, constitutive model*

## 1  Introduction and basic concept

A considerable displacement of structures may be caused by the accumulation of irreversible strains in the soil due to cyclic loading. If the number of cycles is large then even relatively small amplitudes may endanger the long-term serviceability of structures, especially if their displacement tolerance is small, e.g. of communication structures like a magnetic levitation train, watergates or wind power plants. Under undrained conditions, in place of the usual densification, excessive pore pressure is generated. It may lead to soil liquefaction and eventually to a loss of the overall stability. Therefore the accumulation phenomenon is of practical importance. This paper deals with the prediction of the accumulation of stress and strain in sand for a large number ($> 10^3$) of small to moderate total strain amplitudes ($< 10^{-3}$). The presented model is based mainly on the laboratory tests carried out by the second author. A more detailed description of the test results and a survey of similar investigations in the literature can be found in [1, 2].

A *cycle* is understood as a path (a trajectory parametrized by time) which is recurrently passed through by the state variables (usually strain or stress) describing the material. Such paths, sometimes referred to as *loops*, are caused by non-monotonic loads. Having plotted a variable ⊔ we may define its *average* value ⊔$^{\mathrm{av}}$ to be the centre of the smallest hypersphere that encompasses all states ⊔ upon the cycle[1]. The amplitude of a scalar variable is defined as ⊔$^{\mathrm{ampl}} = \max|⊔ - ⊔^{\mathrm{av}}|$. A *tensorial* definition of the strain amplitude is proposed in Section 3. It describes not only the size but also the polarization and the ovality of a cycle.

It turns out that the phenomenon of accumulation depends strongly on several subtle properties of soil like distribution of grain contact normals, arrangement of grains etc, which cannot be expressed by the customary state variables (stress and void ratio) only. Two new state variables are therefore proposed: the cyclic preloading $g^A$ which memorizes the amount of fatigue loading in the past and the back-polarization $\boldsymbol{\pi}$ memorizing the orientation of the recent cycles. These variables are discussed in more detail in Sections 2.4 and 3.2, respectively.

The phenomenon of *accumulation* consists in a summation of small residual strains (pseudo-creep) or residual stresses (pseudo-relaxation). For the two-dimensional case it is shown schematically in Figure 1. If stress cycles are applied, Figure 1a, we observe cyclic pseudo-creep and if strain cycles are applied, Figure 1b, we obtain cyclic pseudo-relaxation. Some tests are mixed-controlled (cf. Section 3.1.3 and 3.2.3 in [3]), so that both, pseudo-relaxation and pseudo-creep, may occur simultaneously, Figure 1c. The unspecified term *accumulation* seems, therefore, to be a convenient term covering the cyclic pseudo-relaxation as well as the cyclic pseudo-creep. We often speak of accumulation in this general sense here, i.e., independently of the technical aspect how an experiment is controlled.

In the simplest case[2] the proposed constitutive relation can be expressed for large deformations by

$$\mathring{\mathbf{T}} = \mathsf{E} : (\mathbf{D} - \mathbf{D}^{\mathrm{acc}}), \tag{1}$$

wherein $\mathring{\mathbf{T}}$ is the Zaremba-Jaumann rate of the Cauchy stress, $\mathbf{D}$ denotes the total stretching, $\mathsf{E}$ is a pressure-dependent (hypo)elastic stiffness and $\mathbf{D}^{\mathrm{acc}}$ is the irreversible stretching caused by cyclic loading or rate of strain accumulation. The notation is explained in Appendix A. Figure 1 interprets $\mathbf{D}^{\mathrm{acc}}$ in differently controlled tests. The number of cycles $N$ is treated as a *continuous* time-like variable, and the material "rate" of ⊔ is understood as $\dot{⊔} = \mathrm{d}⊔/\mathrm{d}N$ here.

Considering the logarithmic strain $\boldsymbol{\epsilon} = \ln \mathbf{U}$, wherein $\mathbf{U}$ denotes the right stretch tensor, we distinguish between *in-phase* (=IP) strain cycles and *out-of-phase* (=OOP) cycles. The IP-cycles can be defined by the equation

$$\boldsymbol{\epsilon} = \boldsymbol{\epsilon}^{\mathrm{av}} + \boldsymbol{\epsilon}^{\mathrm{ampl}} f(t), \tag{2}$$

wherein $\boldsymbol{\epsilon}^{\mathrm{ampl}}$ contains the amplitudes of the individual components, i.e. $(\boldsymbol{\epsilon}^{\mathrm{ampl}})_{ij} = (\epsilon_{ij})^{\mathrm{ampl}}$. All components of $\boldsymbol{\epsilon}$ given by (2) oscillate together according to the same scalar periodic function, e.g. $f(t) = \sin(t)$ which is varying between -1 and 1. IP-cycles that have only one non-zero eigenvalue of $\boldsymbol{\epsilon}^{\mathrm{ampl}}$ are termed *uniaxial*, otherwise they are *multiaxial*.

The out-of-phase (=OOP) cycles do not cannot be expressed by (2), e.g.

$$\boldsymbol{\epsilon}(t) = \boldsymbol{\epsilon}^{\mathrm{av}} + \begin{pmatrix} \epsilon_{11}^{\mathrm{ampl}}\sin(t) & 0 & 0 \\ 0 & \epsilon_{22}^{\mathrm{ampl}}\sin(t+\theta) & 0 \\ 0 & 0 & 0 \end{pmatrix}. \tag{3}$$

---

*Institute of Soil Mechanics and Foundation Engineering, Ruhr-University Bochum, Gebaeude IA 4/30, Universitaetsstrasse 150, D-44801 Bochum, Phone: +49 (0234) 32 260 79, Fax: +49 (0234) 32 141 50, E-Mail: Andrzej.Niemunis@rub.de

†Institute of Soil Mechanics and Foundation Engineering, Ruhr-University Bochum

‡Institute of Soil Mechanics and Foundation Engineering, Ruhr-University Bochum

[1]A slightly different definition of ⊔$^{\mathrm{av}}$ could be the middle point between the two most distant states. Such definition leads to a more efficient numerical implementation.

[2]In an FE implementation or if the cyclic loading is accompanied by monotonic loading (5) must be used instead of (1)
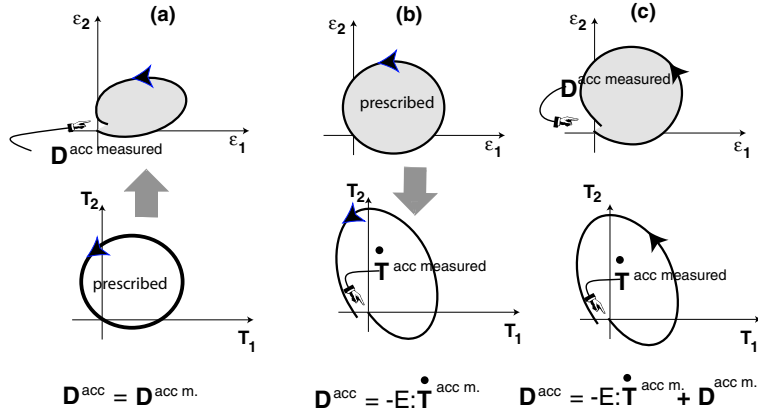
Figure 1:
(a) *Stress cycles (= all stress components are prescribed and the stress loop is perfectly closed) leave residual strains.*
(b) *Strain cycles leave residual stresses.*
(c) *Mixed control tests leave both residual stresses and residual strains.*
*Pure accumulation (not superposed by monotonic loading) is considered and therefore $\mathbf{D}^{\mathrm{pl}}$ can be disregarded. The superscript $\sqcup^{m\cdot}$ stands for 'measured'.*

Due to the phase shift $\theta \neq n\pi$, the OOP strain loop (3) encloses some area in the strain space (the shadowed area(s) in Figure 1). The shape of a strain cycle is of importance for the accumulation (similarly as for the fatigue of metals [4,5]). Quantifying the OOP-cycles (Section 3) one should account for the rotation of the principal strain axes within a cycle but disregard the rigid body rotation. This is done if the strain $\boldsymbol{\epsilon}$ is calculated with respect to the material frame of reference. In the presented model the logarithmic strain is defined with respect to the initial material configuration (usually $K_0$-state) as

$$\boldsymbol{\epsilon} = \ln \mathbf{U} = \mathbf{R}^T \cdot \ln \mathbf{V} \cdot \mathbf{R}, \qquad (4)$$

wherein $\mathbf{V}$ and $\mathbf{U}$ denote the left and the right stretch tensor and $\mathbf{R}$ is the rotation tensor appearing in the polar decomposition of the deformation gradient[3].

Displacements of structures due to cyclic loading are often predicted using *settlement formulae*, e.g. [6,7]. The settlement $s(N)$ after $N$ cycles is extrapolated from the residual settlement $s_1$ after the first cycle. Various empirical functions, e.g. $s(N) = s_1 N^C$ or $s(N) = s_1(1 + C \ln N)$ with a material constant $C$, were proposed in the literature. In this paper, we argue that the accumulation depends on numerous factors, see Section 2, which are too complicated to be lumped together into a single parameter $s_1$. Moreover, most of the popular settlement formulas are self-contradictory (inconsistent), as demonstrated in Appendix B.

## 1.1 Explicit vs conventional constitutive model

Predicting the accumulation due to cyclic loading we may choose between two computational strategies: *implicit* or *explicit*[4] one. The conventional (= implicit) models describe each loop using many strain increments. The accumulation of stress or strain appears as a by-product of such calculation resulting from the fact that the strain or stress loops are not perfectly closed (accumulation is implied) . Elastoplastic models with a single yield surface are not suitable for the implicit approach because they predict no irreversible strain in the elastic regime. Usually more sophisticated (e.g. endochronic [8] or multi-surface [9–11]) constitutive formulations are used. Their practical applicability, however, is limited by the number of cycles. During

an application of a large number of cycles some inevitable cumulative errors may become important. They may be caused by the numerical implementation, by too large time steps, by a non-conservative (*hypo*elastic) reversible part of the stress - strain relation, etc. An example of a numerical error is a drift of the average stress caused by the inaccuracy of the Euler forward integration, Figure 2. A considerable change of stress can be seen after 1000 perfectly closed strain loops (calculated with 360 increments per loop) although the material model is hyperelastic and no accumulation of stress should theoretically appear. A perusal of a single (and seemingly closed) stress loop would reveal that it has actually a small gap due to the inaccurate integration. This systematic error is accumulated so that the final (1000th) loop is shifted diagonally in Figure 2. Even using 3600 increments per cycle the error is still considerable. The multi-surface plasticity models are not free from similar
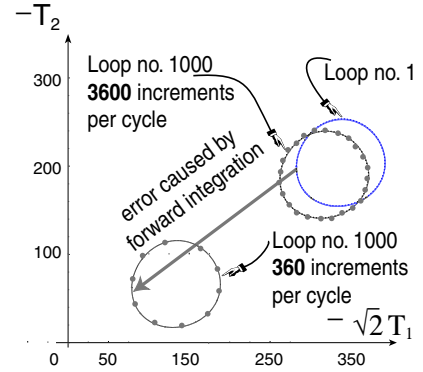


Figure 2: *Accumulation of numerical error due to explicit (Euler forward) time integration. Theoretically no stress accumulation should be obtained in hyperelastic materials after a closed strain path. Euler backward integration causes an analogous error in the opposite direction.*

systematic errors. They become evident if the number of cycles $N$ is large. For example, $10^5$ cycles with 100 increments per each cycle may magnify systematic errors $10^7$-times! This requires a constitutive model of an unreachable perfection.

The high-cycle model proposed in this paper is based on an alternative idea which is referred to as an *explicit* or *N-type* formulation. Explicit models [**?**,12–26] are similar to the viscoplastic ones in which in place of time $t$ the number $N$ of cycles is used. The accumulation of strain due to a package
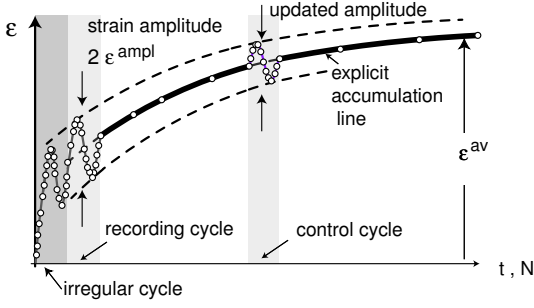
---

[3]We had to 'unrotate' the total strain because it is defined as $\ln \mathbf{V}$ in the FE program ABAQUS.
[4]Euler forward/backward integration is not meant here.

Figure 3: *The basic idea of explicit calculation of the cumulative deformation.*

of $\Delta N$ cycles of a given amplitude is predicted directly. For example, an increment of $\Delta N = 25$ cycles with the amplitude $\epsilon^{\mathrm{ampl}} = 10^{-4}$ results in an irreversible strain $\mathbf{D}^{\mathrm{acc}}\Delta N$ wherein $\mathbf{D}^{\mathrm{acc}}$ is given by the explicit formula (7). As we shall see, this is the essential equation of the presented model. It is based on numerous tests on medium coarse uniform sand.

The following flowchart, with reference to Figure 3, shows how an explicit FE program works.

1. Calculate the initial stress field (from self weight and all monotonic loads) using a conventional, e.g. multi-surface plasticity model. It is not recommendable to calculate the initial stress with an elastic model because it does not guarantee that the resulting initial stress will lie within the admissible stress range (e.g. defined by Matsuoka and Nakai [27]).
2. Calculate implicitly at least two first load cycles using a multi-surface plasticity model or, as we do, the extended hypoplasticity model [28]. The "small strain" nonlinearity of soil should be accounted for.
3. Record the logarithmic strain path during the second cycle (=first regular cycle) at each integration point.
4. Evaluate the *tensorial strain amplitude* $\mathsf{A}_\epsilon$ (a fourth-order tensor $\mathsf{A}_\epsilon \neq \boldsymbol{\epsilon}^{\mathrm{ampl}}$) from the recorded strain path, see Section 3. The amplitude is assumed constant over all subsequent cycles, until it is recalculated in a so-called control cycle[5].
5. Find the accumulation rate $\mathbf{D}^{\mathrm{acc}}$ of strain using (7). In the subsequent cycles only the general trend of the accumulation is calculated. This trend is depicted with the thick line in Figure 3.
6. Find the Zaremba-Jaumann rate of the Cauchy stress

$$\mathring{\mathbf{T}} = \mathsf{E} : (\mathbf{D} - \mathbf{D}^{\mathrm{acc}} - \mathbf{D}^{\mathrm{pl}}) \qquad (5)$$

and the stress increment $\Delta\mathbf{T} = \mathring{\mathbf{T}}\Delta N$ caused by a package of $\Delta N$ cycles (= a single increment of the fatigue load). The plastic strain rate $\mathbf{D}^{\mathrm{pl}}$ may appear if a monotonic loading is applied simultaneously with the fatigue loading. The Matsuoka and Nakai [27] yield condition (M-N) with the associated flow rule is used to calculate $\mathbf{D}^{\mathrm{pl}}$. The rate $\mathbf{D}^{\mathrm{acc}}$ can be calculated first and used in the modified elastoplastic loading criterion

$$\mathbf{n} : \mathsf{E} : (\mathbf{D} - \mathbf{D}^{\mathrm{acc}}) > 0, \qquad (6)$$

wherein $\mathbf{n}$ denotes the outer normal direction to the M-N yield surface. The advantage of (5) over (1) is explained in Section 2.2. The isotropic hypoelastic stiffness $\mathsf{E}$ with a constant Poisson's ratio ($\approx 0.2$) and with a pressure dependent Young modulus ($\sim (p/p_{\mathrm{atm}})^{2/3}$) is used in (5). The *hyper*elasticity is not obligatory in the explicit formulations but it is of great importance [30] for implicit models[6].

The FE program redistributes stress in the course of equilibrium iteration and, depending on the boundary conditions, the accumulation results in settlements or in pseudo-relaxation. It is advisable to interrupt occasionally this accumulation procedure by so-called *control cycles*, Figure 3, calculated implicitly in order to recalculate the strain amplitude which may change due to a redistribution of stress or a reduction of the void ratio. The admissibility of the stress state (which may get lost, e.g., due to a large isotropic relaxation under undrained conditions) is also tested.

Numerous explicit constitutive models have been proposed in the literature [12–26]. They are usually strongly simplified because the required cyclic testing is very laborious and it is difficult to collect a sufficient amount of experimental data to cover a large range of the material behaviour. Many models are focussed on a very specific practical application only. In this paper a systematic and general study of the high-cycle modelling of soil is attempted.

## 2  Elements of the model

As already mentioned, the essential part of the presented explicit model is the formula (7) for the rate of strain accumulation $\mathbf{D}^{\mathrm{acc}}$. We have a good reason for expressing the accumulation (in a general sense) with the strain rate $\mathbf{D}^{\mathrm{acc}}$ and not with the stress rate $\mathring{\mathbf{T}}^{\mathrm{acc}}$, let alone the accumulated pore pressure. The advantage of $\mathbf{D}^{\mathrm{acc}}$ over the pseudo-relaxation and the pore pressure generation is that it need *not* vanish with the effective stress, i.e. for $\mathbf{T} = \mathbf{0}$. This phenomenon is illustrated in Figure 4. On top of that, the pore pressure build-up
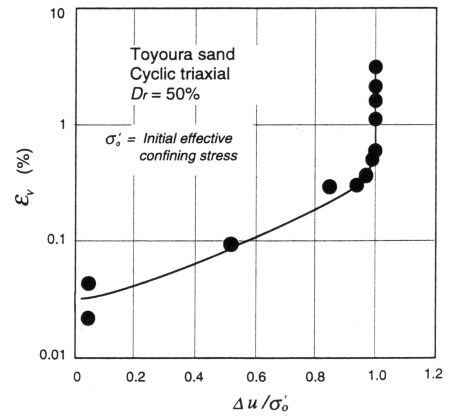


Figure 4: *Experimental evidence that the accumulation of strain continues also at vanishing effective stress $\mathbf{T} = \mathbf{0}$, see [31]. During cyclic loading under undrained conditions the excess pore pressure $\Delta u$ increases up to the initial effective stress $\sigma_0$. Then all components of the effective stress must vanish (the soil is liquefied). The additional increase of volumetric strain from $\epsilon_v = 0.5\%$ to $\epsilon_v = 4\%$, measured during the subsequent isotropic reconsolidation, indicates that the soil skeleton must have been latently densifying in the liquefied stage, i.e. for $\mathbf{T} = \mathbf{0}$.*

---

[5]Alternatively the strain amplitude can be directly measured in situ [29] or evaluated from a separate, e.g. dynamic calculation. During the first 100-1000 cycles several fresh pluviated samples subjected to relatively large constant stress amplitudes (reaching 25° mob. friction angle) were observed to stiffen. This stiffening (even by 15%, [1]) during the so-called *conditioning phase* cannot be explained by changes in the density, in the stress or in the geometry of the sample only. The phenomenon of stiffening has not been considered in the hypoplastic model as yet. This effect is included, however, in the factor $f_N$ used in the explicit formula (7) for $\mathbf{D}^{\mathrm{acc}}$.

[6]A *hypo*elastic model does not guarantee that a closed stress path results in a closed strain path and it is refutable from the thermodynamic point of view (enables a perpetuum mobile of the second kind).

is unsuitable because it describes merely the isotropic part of the pseudo-relaxation.

It has been demonstrated experimentally that $\mathbf{D}^{\mathrm{acc}}$ depends on a number of factors which can be treated independently within the examined range [1, 2, 32–34]. and which can be combined into the following product

$$\mathbf{D}^{\mathrm{acc}} = \mathbf{m} \, f_{\mathrm{ampl}} \ \dot{f}_N \ f_p \ f_Y \ f_e \ f_\pi. \qquad (7)$$

The functions $f_{\mathrm{ampl}}$, $\dot{f}_N$, $f_p$, $f_Y$, $f_e$ and $f_\pi$ describe the influence of the strain amplitude $\epsilon^{\mathrm{ampl}}$, the number of cycles $N$, the average mean pressure $p^{\mathrm{av}}$, the average stress ratio, the void ratio $e$, and the change of the polarization of the strain loop, respectively. The validity of the above empirical formula has been checked within the range of performed tests. The amplitudes were varied within the range $5 \cdot 10^{-5} < \epsilon^{\mathrm{ampl}} < 5 \cdot 10^{-3}$ and the average stresses between $50 \leq p^{\mathrm{av}} \leq 300$ kPa for triaxial compression as well as for triaxial extension. In the following subsections the components of (7) are discussed.

## 2.1 Direction of accumulation m

The accumulation $\mathbf{D}^{\mathrm{acc}}$ has a volumetric portion but also a significant deviatoric component [1, 25]. Since the ratio between the deviatoric and the volumetric accumulation has been observed to be almost constant for a given stress $\mathbf{T}^{\mathrm{av}}$, Figure 5, it seems reasonable to define a kind of flow rule $\mathbf{m}(\mathbf{T}^{\mathrm{av}}) = \vec{\mathbf{D}}^{\mathrm{acc}}$. The unit tensor $\mathbf{m}$ points in the direction of accumulation in the strain space. The resulting coaxiality between $\mathbf{D}^{\mathrm{acc}}$ and
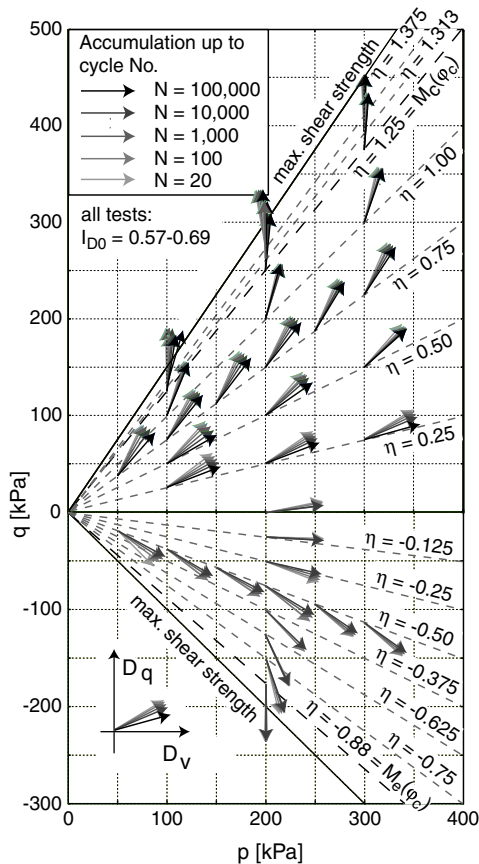


Figure 5: *Directions $\mathbf{m}$ of strain accumulation were determined from numerous cyclic triaxial tests for various stress ratios $\eta^{\mathrm{av}} = q^{\mathrm{av}}/p^{\mathrm{av}}$. The initial index of density of a sample is denoted by $I_{D0}$.*

$\mathbf{T}$ is analogous to the coaxiality of $\mathbf{D}^{\mathrm{pl}}$ and $\mathbf{T}^{\mathrm{av}}$ in the plasticity theory. The direction $\mathbf{m}$ has been found independent of

the void ratio $e$, of the amplitude $\epsilon^{\mathrm{ampl}}$ and of the polarization $\vec{\mathsf{A}}_\epsilon$ defined in Section 3. The flow rule may slightly vary with increasing number of cycles $N$, Figure 5, but this fact has been disregarded in the present version of the model. Judging by the triaxial tests presented in Figure 5, the direction of accumulation $\mathbf{m}$ is well approximated by the associated flow rule

$$\mathbf{m} \sim -\frac{1}{3}\left(p - \frac{q^2}{M^2 p}\right) \mathbf{1} + \frac{3}{M^2}\mathbf{T}^* \qquad (8)$$

from the modified Cam-clay model [35] with the Roscoe's invariants $p, q$ and the critical state line inclined at $M = \frac{6 \sin \varphi_c}{3 \pm \sin \varphi_c}$. The experiments [1] show that the accumulation is dilative beyond the critical state line, $|q/p| > M$, which is in accordance with (8).

## 2.2 Cumulative and plastic strains

The plastic stretching $\mathbf{D}^{\mathrm{pl}}$ caused by monotonic loading and the cumulative stretching $\mathbf{D}^{\mathrm{acc}}$ are treated separately in (5), although from the physical point of view they cannot be distinguished. The decomposition of the irreversible strain rate into $\mathbf{D}^{\mathrm{pl}}$ and $\mathbf{D}^{\mathrm{acc}}$ is forced by the explicit strategy of calculation. Implicit models need not such separation.

To understand the usefulness of $\mathbf{D}^{\mathrm{pl}}$ it is instructive to consider a simple 1-dimensional example with a rod made of a tension cut-off material and fixed at both ends. During a cooling process (= thermic shrinkage) tensile stress may occur. However, since no tension is allowed for, the plastic strains are indispensable. In other words, a constitutive model of the form $\dot{T} = E(D - D^{\mathrm{thermic}} - D^{\mathrm{pl}})$ is required and $\dot{T} = E(D - D^{\mathrm{thermic}})$ is insufficient. At first, one could expect that unlike the thermic deformation, the fatigue loading does not require plastic strains because pseudo-relaxation nudges the stress inward the yield surface. Inferring from element tests, the stress paths could not surpass the Matsuoka and Nakai yield surface in the process of pseudo-relaxation because the flow rule $\mathbf{m}$ points to the outside of the yield surface, Figure 5, and therefore the relaxation $\overset{\circ}{\mathbf{T}}^{\mathrm{acc}} = -\mathsf{E} : \mathbf{D}^{\mathrm{acc}}$ tends inwards. However, the absence of $\mathbf{D}^{\mathrm{pl}}$ does lead to severe problems in FE calculations! Tension or excessive stress ratios may appear if cyclic loading is superposed by a simultaneous monotonic loading which enforces a plastification. Even in boundary value problems under a purely fatigue loading but with a strongly *inhomogeneous* spatial distribution of the accumulation rate (1) can inflict excessive shear or tensile stresses. For example, it is the case if an element that experiences little or no direct fatigue loading itself had a strongly loaded neighbour. The plastic rate $\mathbf{D}^{\mathrm{pl}}$ would be indispensable in the weakly loaded element to make it compliant with the large deformation outside.

## 2.3 Scalar value of the amplitude

The rate of accumulation depends essentially on the amplitude which enters (7) via $f_{\mathrm{ampl}}$. The factor $f_{\mathrm{ampl}}$ describes the influence of the size (= scalar value) of the amplitude which is $\epsilon^{\mathrm{ampl}} = \|\boldsymbol{\epsilon}^{\mathrm{ampl}}\|$ for IP-cycles and $\epsilon^{\mathrm{ampl}} = \|\mathsf{A}_\epsilon\|$ for OOP-cycles (Section 3). Figure 6 shows that the accumulation rate is proportional to the square of the strain amplitude. This proportionality is valid up to $\epsilon^{\mathrm{ampl}} = 10^{-3}$. A few tests with very large amplitudes show that the accumulation rate remains almost constant above this limit. Therefore we propose

$$f_{\mathrm{ampl}} = \begin{cases} \left(\dfrac{\epsilon^{\mathrm{ampl}}}{\epsilon_{\mathrm{ref}}^{\mathrm{ampl}}}\right)^2 & \text{for } \epsilon^{\mathrm{ampl}} \leq 10^{-3} \\ 100 & \text{otherwise}, \end{cases} \qquad (9)$$
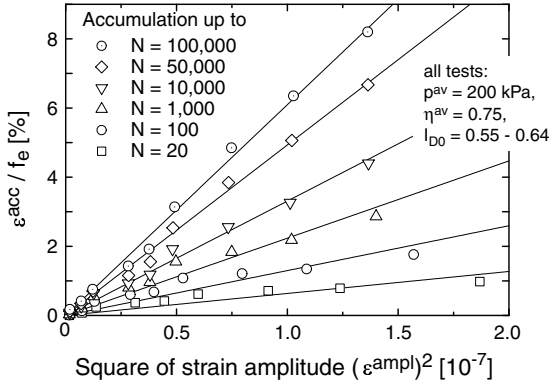
4

Figure 6: *The rate of accumulation is proportional to the square of the strain amplitude. The diagram has been purified from the variability of $f_e$.*

wherein the reference amplitude is $\epsilon_{\mathrm{ref}}^{\mathrm{ampl}} = 10^{-4}$. Equation (9) has been found valid for the range $5 \cdot 10^{-5} < \epsilon^{\mathrm{ampl}} < 5 \cdot 10^{-3}$.

In some publications [20, 36] (including our recent conference paper [2], alas) the volumetric portion $\epsilon_P^{\mathrm{ampl}}$ of the amplitude is reported to have less influence on the rate of accumulation than the deviatoric one $\epsilon_Q^{\mathrm{ampl}}$. The isomorphic strain components $\epsilon_P^{\mathrm{ampl}}$ and $\epsilon_Q^{\mathrm{ampl}}$ are defined in Appendix A. However, careful reinterpretation of our tests considering the membrane penetration effect [37] has revealed that $\epsilon_P^{\mathrm{ampl}}$ and $\epsilon_Q^{\mathrm{ampl}}$ contribute equally(!) to the accumulation and need not be treated separately. Hence, $\epsilon^{\mathrm{ampl}} = \sqrt{\left(\epsilon_Q^{\mathrm{ampl}}\right)^2 + \left(\epsilon_P^{\mathrm{ampl}}\right)^2}$ can be directly substituted into (9).

We have chosen to quantify the magnitude of a cycle in terms of the strain amplitude $\epsilon^{\mathrm{ampl}}$ rather than of the stress amplitude $T^{\mathrm{ampl}}$ for three reasons. Firstly, $T^{\mathrm{ampl}}$ does not provide the sufficient information about large amplitudes. From $T^{\mathrm{ampl}}$ alone one cannot distinguish between the cycles that are just touching the yield surface and those which penetrate the plastic region, Figure 7. They have the same stress amplitude but very different strain amplitudes and cause different accumulations. Secondly, a usage of $T^{\mathrm{ampl}}$ would require a reformulation of $f_p$ (Section 2.5) making it stronger barotropic ($p$-dependent). This would be numerically disadvantageous. Thirdly, $T^{\mathrm{ampl}}$ vanishes at the limit $\mathbf{T}^{\mathrm{av}} = \mathbf{0}$, hence the phenomenon presented in Fig. 4 would be omitted.

The amplitude evaluated from the first (=*irregular*) cycle is often untypical. As illustrated in Figure 8a, the strain amplitude obtained from an irregular stress-controlled cycle is too large. Moreover an irregular strain-controlled cycle, Figure 8b, commenced at $q^{\mathrm{av\ ini}}$ may strongly affect the average stress, $q^{\mathrm{av\ ini}} \to q^{\mathrm{av}}$. The subsequent pseudo-relaxation is much slower.

As already mentioned, the applicability of high-cycle models is restricted to relatively small amplitudes, $\epsilon^{\mathrm{ampl}} < 5 \cdot 10^{-3}$. For larger amplitudes alternating plasticity may occur and the rate of strain accumulation $\mathbf{D}^{\mathrm{acc}}$ (including direction $\mathbf{m}$) depends essentially on the asymmetry of the strain loop. In such case the description given by (8) and (9) becomes inaccurate. Similarly, for stresses in the vicinity of the yield surface, even relatively small strain cycles may cause the progressive failure which is an accumulation much faster than the one described by (9). For these reasons the FE routine should control whether the yield surface is encountered during the implicit calculation (item 2 in the flowchart in Section 1.1) or not. If so, (9) is not applicable and the residual strain $\mathbf{D}^{\mathrm{acc}}$ should be *directly extrapolated*. This means that the estimation (7) is replaced

by $\mathbf{D}^{\mathrm{acc}} = \mathbf{D}^{\mathrm{acc\ m}} - \mathsf{E} : \overset{\circ}{\mathbf{T}}{}^{\mathrm{acc\ m}}$, wherein the recorded residuals are denoted with superscript $\sqcup^{\mathrm{m}}$, cf. Figure 1c.

## 2.4 Cyclic history

The phenomenon of accumulation due to a given cyclic loading cannot be described solely by the stress $\mathbf{T}$ and the void ratio $e$. The rate of accumulation depends also on the cyclic history, i.e. on the number and the size of cycles applied in the past. Presumably a static preloading is also of importance [38]. The
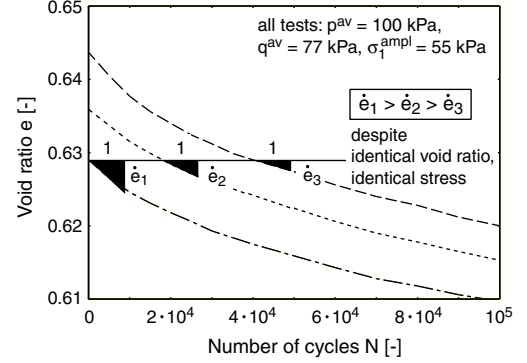


Figure 9: *The effect of cyclic loading history on the rate of densification $\dot{e} = \mathrm{d}e/\mathrm{d}N$ measured during cyclic drained triaxial test.*

effect of cyclic preloading is strong and should not be disregarded. Figure 9 shows the compaction curves of three triaxial samples which have different densification rates $\dot{e}$ (rates of change of the void ratio $e$) passing through the same void ratio $e = 0.629$. The average stress and the amplitude are identical so that the only reason for the observed difference can be the cyclic preloading which renders the accumulation slower.

In order to consider the cyclic preloading two additional state variables have been introduced: the scalar $g^A$ for the number of cycles $N$ and their size $\epsilon^{\mathrm{ampl}}$ and the tensor $\boldsymbol{\pi}$ for the recent polarization. Both state variables are phenomenological, i.e. we do not investigate whether they are related to the number of grain contacts and their directional distribution, the spatial fluctuation of stress, internal systems of shear bands etc. The major disadvantage of non-physical state variables is that they cannot be directly measured. They must be estimated by their effects. In particular, the initial *in-situ* value of $g^A$ can be correlated [34] to the liquefaction potential [39]. The discussion of $\boldsymbol{\pi}$ is deferred until Section 3 and we continue with the scalar state variable $g^A$ here.

Using a freshly pluviated sand sample, the cyclic history (number and size of all applied cycles) is known. If the number of cycles in the past was large than the accumulation rate is slower. For strain cycles of constant amplitude, the increase of the total strain accumulated after $N$ cycles, see Figure 10, can be well approximated by the empirical formula

$$f_N = C_{N1} \left[\ln\left(1 + C_{N2}N\right) + C_{N3}N\right] \qquad (10)$$

with three material constants $C_{N1}, C_{N2}$ and $C_{N3}$ (the latter is important for large numbers of cycles only). Equation (10) has already been purified from the concurrent effects due to changes in the void ratio, stress, etc. The *rate* of accumulation decreases with $N$ proportionally to the derivative of (10),

$$\dot{f}_N = C_{N1} \left[\frac{C_{N2}}{1 + C_{N2}N} + C_{N3}\right]. \qquad (11)$$

Unfortunately, as we shall see, the product of $f_{\mathrm{ampl}}$ and $\dot{f}_N$ given by (9) and (11) severely contradicts the Miner's rule [40].
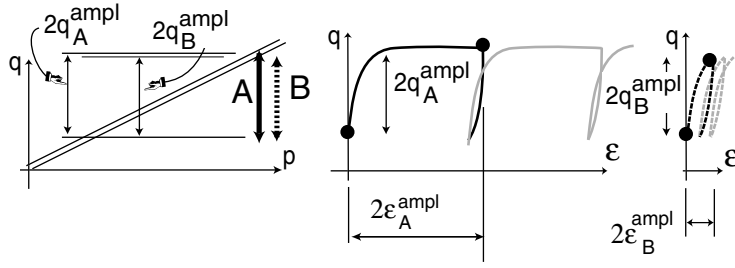
Figure 7: *Unsymmetric stress-controlled cycles. The large cycles A (solid line) which encounter the yield surface (double line) are poorly described by the stress amplitude $q_A^{\mathrm{ampl}}$ alone. The stress path B (dotted line) which approaches only the yield surface without touching it has almost the same stress amplitude $q_B^{\mathrm{ampl}} \approx q_A^{\mathrm{ampl}}$ but the respective strain amplitudes are quite different and so are the rates of accumulation.*
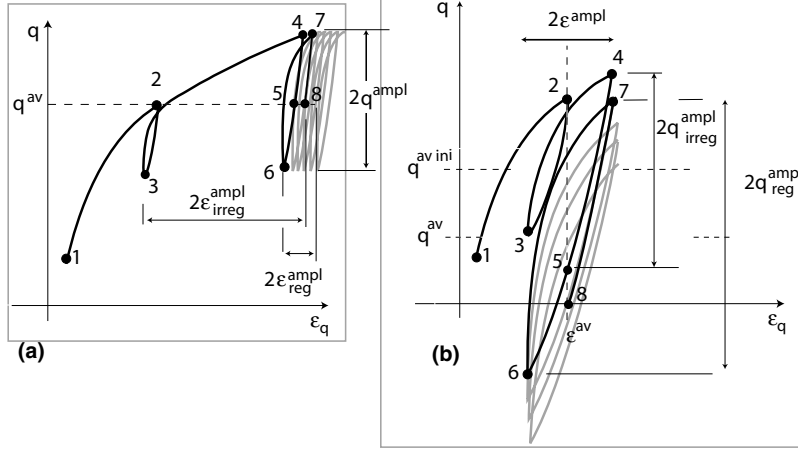


Figure 8: *(a) Unsymmetric stress-controlled cycles. (b) Unsymmetric strain-controlled cycles. Monotonic loading 1-2 is followed by the irregular cycle (2-3-4-5) and the regular cycle (5-6-7-8). In the irregular stress-controlled cycle the strain amplitude $\epsilon_{\mathrm{irreg}}^{\mathrm{ampl}}$ is too large. In the irregular strain-controlled cycle the stress amplitude is too small and, which is more important, the average stress changes from $q^{\mathrm{av\ ini}}$ to $q^{\mathrm{av}}$.*
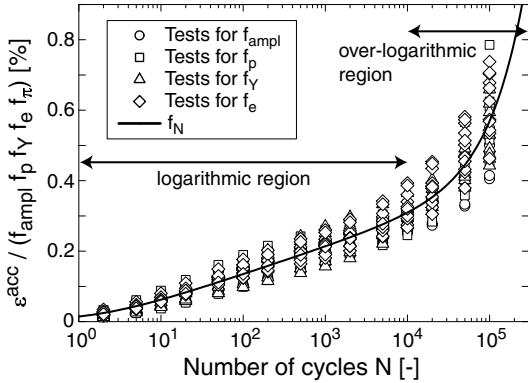


Figure 10: *Accumulated strain $\varepsilon^{\mathrm{acc}}$ divided by the functions $f_{\mathrm{ampl}}$, $f_p$, $f_Y$, $f_e$ and $f_\pi$ as a function of the number of cycles.*

Originally the Miner's rule pertains to the fatigue of metals and generalizes the Wöhler's curve. The Wöhler's SN-curve shows the number $N_f$ of uniaxial cycles with a stress amplitude $S = T_1^{\mathrm{ampl}} = $ const that causes failure. The (Palmgren-)Miner's rule describes an analogous condition for several blocks of cycles with constant amplitudes within each block. Suppose we have $n$ blocks of cycles. In the $i$-th block the number of actually applied cycles is $N_i$ and their amplitude $A_i$ is constant. Suppose also that we know the numbers $N_{fi}$ of cycles to failure for each amplitude $A_i$. The Miner's rule excludes failure if

inequality

$$\sum_{i=1}^{n} \frac{N_i}{N_{fi}} < 1 \qquad (12)$$

is satisfied. The Miner's rule implies that:

- the sequence of application of constant-amplitude blocks is of no importance,

- the periodic strain loop can be decomposed into several *convex* loops (e.g., using the so-called rainflow algorithm). These convex loops can be applied sequentially as separate blocks with constant amplitudes.

It is controversial whether sands obey the Miner's rule very rigorously. However, in one case the inconsistency between (11) and the Miner's rule is unacceptable, namely for a combination of a package of $N_1$ cycles with $\epsilon_{(1)}^{\mathrm{ampl}}$ and a package of $N_2$ cycles with almost vanishing amplitude $\epsilon_{(2)}^{\mathrm{ampl}} \approx 0$. The total accumulation should be independent of the sequence of application of these packages because it does not matter whether we *do nothing* after or before the actual loading with $\epsilon_{(1)}^{\mathrm{ampl}} > 0$. The vanishingly small cycles should have no effect at all. However, (11) unwisely disregards the sizes of amplitudes *in the past*.

A state variable memorizing the number of cycles together with their amplitudes is therefore required. Though a simple concept [20] of using the product $\left(\epsilon^{\mathrm{ampl}}\right)^2 N$ instead of $N$ in (11)
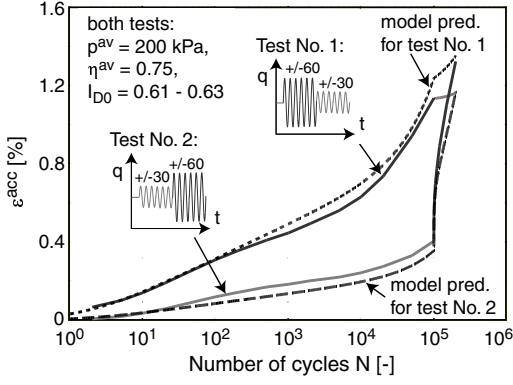
Figure 11: *Numerical calculation and experimental verification of the Miner's rule.*

obeys the Miner's rule, it is in conflict with (9), cf. [32]. The variable $g^A$, proposed in the following, is a compromise solution. We consider the product of $f_{\text{ampl}}$ and $\dot{f}_N$ denoting it as $\dot{g} = f_{\text{ampl}} \, \dot{f}_N$. Functions $f_{\text{ampl}}$ and $\dot{f}_N$ are further on given by (9) and (11). Note that only a part of $\dot{g}$ depends on $N$ namely $\dot{g}^A = f_{\text{ampl}} C_{N1} C_{N2}/(1 + C_{N2} N)$. Integrating $\dot{g}$ with respect to $N$ one obtains

$$g = \overbrace{f_{\text{ampl}} C_{N1} \ln\left(1 + C_{N2} N\right)}^{=g^A} + \overbrace{f_{\text{ampl}} C_{N1} C_{N3} N}^{=g^B} \quad (13)$$

The idea is to reformulate (11) replacing $N$ by $g^A$. For this purpose we solve $g^A = g^A(N)$ for $N$ and substitute the result into the expression for $\dot{g}$, viz.

$$\dot{g} = f_{\text{ampl}} C_{N1} C_{N2} \exp\left(-\frac{g^A}{C_{N1} f_{\text{ampl}}}\right) + f_{\text{ampl}} C_{N1} C_{N3}, \quad (14)$$

wherein $f_{\text{ampl}}$ refers to the current amplitude and $g^A$ contains the information about the past amplitudes and the respective numbers of cycles. By this expedient the Miner's rule is satisfied at the limit of very small amplitudes and (11) remains valid for the special case of $\epsilon^{\text{ampl}} = \text{const}$.

A numerical simulation of the accumulation caused by two blocks of cycles with different amplitudes and applied in different sequences gives almost the same total accumulation, so it is in agreement with the Miner's rule and with the experiment, see Figure 11.

## 2.5 Average stress and void ratio

The rate of accumulation depends on the average stress ratio $\hat{\mathbf{T}}^{\text{av}} = \mathbf{T}^{\text{av}}/\text{tr}\left(\mathbf{T}^{\text{av}}\right)$, on the average mean stress $p^{\text{av}}$ and the void ratio $e$. It turns out that one can treat these effects separately and use the product $f_Y \, f_p \, f_e$ of the respective functions. As it might be expected, the rate of accumulation increases with the stress obliquity, especially if the yield surface is approached. This dependence, Figure 12, can be approximated by

$$f_Y = \exp(C_Y \bar{Y}^{\text{av}}) \quad \text{with} \quad C_Y \approx 2 \quad (15)$$

wherein

$$\bar{Y} = \frac{Y - 9}{Y_c - 9}, \qquad Y = -\frac{I_1 I_2}{I_3} \quad \text{and} \quad Y_c = \frac{9 - \sin^2 \varphi_c}{1 - \sin^2 \varphi_c}. \quad (16)$$

The stress invariants $I_1, I_2, I_3$ are functions of $\hat{\mathbf{T}}^{\text{av}}$ defined in Appendix A and the critical friction angle is denoted by $\varphi_c$.

The accumulation rate becomes smaller(!) with $p^{\text{av}}$. The experimental results, Figure 13, can be approximated by

$$f_p = \exp\left[-C_p \left(\frac{p^{\text{av}}}{p_{\text{atm}}} - 1\right)\right] \quad (17)$$

wherein $p_{\text{atm}} = 100$ kPa and the material constant is $C_p \approx 0.43$. The validity of (15) and (17) has been tested for $50 \leq p^{\text{av}} \leq 300$ kPa. Of course, loose sands can be compacted easier than dense ones. This is confirmed by experimental results, Figure 14, which can be approximated by

$$f_e = \frac{(C_e - e)^2}{1 + e} \frac{1 + e_{\text{ref}}}{(C_e - e_{\text{ref}})^2} \quad (18)$$

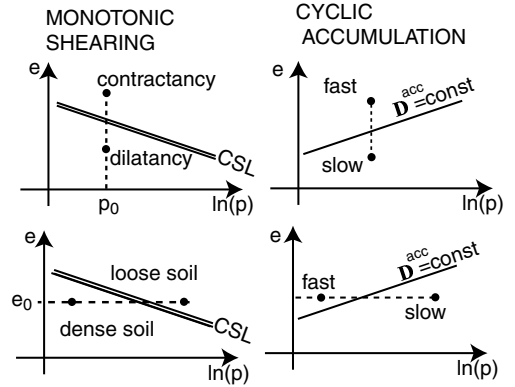with the material constants $e_{\text{ref}} = 0.874$ and $C_e = 0.54$. The



Figure 15: *Lines of constant rate of accumulation in the $e - \ln p$ diagram are differently inclined than the CSL. The notions 'loose' and 'dense' are pressure-dependent in the critical state soil mechanics. For cyclic accumulation this dependence is not analogous.*

factors $f_p f_e$ cannot [32] be described using the 'distance to the critical state line' in the $e - \ln p$ diagram. For a given void ratio $e$, sand contracts faster under monotonic shearing when $p$ is larger. Under cyclic loading it is vice versa, see Figure 15.

## 2.6 Sensitivity of $\mathbf{D}^{\text{acc}}$

In the previous sections we have presented various factors that influence the rate of accumulation. They have been examined in the laboratory and, one by one, approximated by simple formulas. A legitimate question is whether all these factors are really necessary in the model, because the determination of the material constants requires a considerable effort[7]. Table 1 summarizes the presented results showing the expected variability of the functions $f_{\text{ampl}}$, $\dot{f}_N$, $f_p$, $f_Y$, $f_e$ and $f_\pi$ for the typical range of input parameters.

Evidently, all presented factors may strongly influence the rate of accumulation and therefore their incorporation into the model seems justified.

## 3 Out-of-phase cycles and polarization

The rate of accumulation depends on various properties of the strain loop including its orientation in the strain space (= polarization) and its ovality (= shape). It is also important how

---

[7]In the continuation of this work we intend to facilitate the determination of the material constants giving correlations to the angularity, asperity and to the grain size distribution.
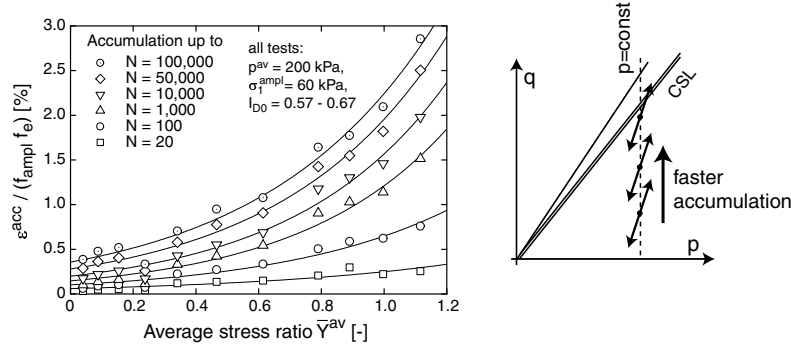
Figure 12: *Accumulated strain $\varepsilon^{\mathrm{acc}}$ as a function of the average stress ratio $\bar{Y}^{\mathrm{av}}$ for different numbers of cycles. The diagrams have been purified from the variability of $f_{\mathrm{ampl}}$ and $f_e$.*
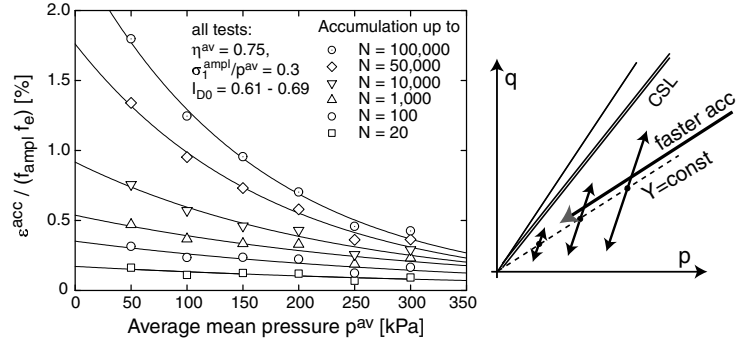


Figure 13: *Accumulated strain $\varepsilon^{\mathrm{acc}}$ in dependence on the average mean pressure $p^{\mathrm{av}}$ for different numbers of cycles. The diagrams have been purified from the variability of $f_{\mathrm{ampl}}$ and $f_e$.*

many dimensions of the strain space are penetrated by the OOP strain cycle.

Practical cases involving OOP cycles are not rare, e.g. Rayleigh waves, moving vehicles, etc. Even during conventional cyclic triaxial tests with a constant cell pressure OOP cycles may (unintentionally) occur due to the variable dilatancy. Unfortunately, OOP cycles cannot be performed easily in the laboratory and they are rarely addressed to in the literature [2, 41].

Our goal is to incorporate the information about the shape and the polarization of the strain loop into the novel *tensorial* definition of the strain amplitude $\mathsf{A}_\epsilon$. It is based on tests performed in the triaxial cell with periodic changes of both, lateral and axial stress. Moreover, several special tests have been done using an extended direct simple shear (DSS) device [2].
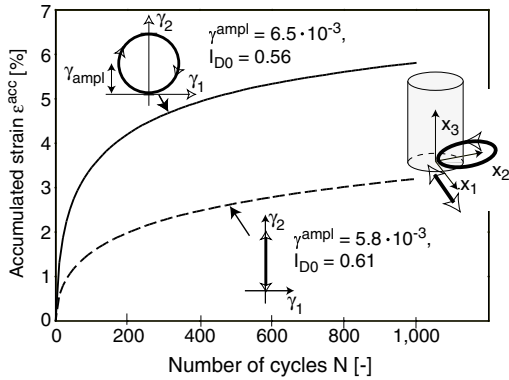


Figure 16: *Circular strain loops generate approximately twice faster accumulation than the in-phase ones.*

## 3.1 Tensorial amplitude $\mathsf{A}_\epsilon$

The OOP cycles produce more accumulation than the IP cycles of the same size, e.g. the accumulation caused by the loop (3) with the phase shift $\theta = 90°$ is larger than the accumulation due to an IP loop of the size $\max(\epsilon_{11}^{\mathrm{ampl}}, \epsilon_{22}^{\mathrm{ampl}})$, see Figure 16. According to several DSS and triaxial tests [2], the accumulation caused by two-dimensional harmonic OOP cycles is equivalent to the total effect of the orthogonal IP cycles into which the strain loop could be decomposed. In particular, the accumulation caused by two-dimensional cycles (3) could be estimated using $f_{\mathrm{ampl}} \sim (\epsilon_{11}^{\mathrm{ampl}})^2 + (\epsilon_{22}^{\mathrm{ampl}})^2$. Analogously, for an OOP cycle

$$\boldsymbol{\epsilon}(t) = \boldsymbol{\epsilon}^{\mathrm{av}} + \begin{pmatrix} \epsilon_{11}^{\mathrm{ampl}} f_{11}(t) & \epsilon_{12}^{\mathrm{ampl}} f_{12}(t) & \epsilon_{13}^{\mathrm{ampl}} f_{13}(t) \\ \epsilon_{21}^{\mathrm{ampl}} f_{21}(t) & \epsilon_{22}^{\mathrm{ampl}} f_{22}(t) & \epsilon_{23}^{\mathrm{ampl}} f_{23}(t) \\ \epsilon_{31}^{\mathrm{ampl}} f_{31}(t) & \epsilon_{32}^{\mathrm{ampl}} f_{32}(t) & \epsilon_{33}^{\mathrm{ampl}} f_{33}(t) \end{pmatrix} \quad (19)$$

with six harmonic functions $f_{ij}(t) = \sin(\omega t + \theta_{ij})$, i.e. with a common period $2\pi/\omega$ but with various phase shifts $\theta_{ij}$, the size of the amplitude can be evaluated from the norm of the matrix composed of the amplitudes, i.e.

$$\epsilon^{\mathrm{ampl}} = \sqrt{\epsilon_{ij}^{\mathrm{ampl}} \epsilon_{ij}^{\mathrm{ampl}}} \quad (20)$$

Note that $\epsilon_{ij}^{\mathrm{ampl}}$ denotes the amplitude of the $ij$-th component of strain, $\epsilon_{ij}^{\mathrm{ampl}} = \max|\epsilon_{ij}(t) - \epsilon_{ij}^{\mathrm{av}}|$ and not the $ij$-th component of a "tensorial amplitude".

Now, a generalization of (20) for arbitrary periodic functions $f_{ij}$ is proposed, i.e. the oscillations need not be harmonic. Moreover, if the accumulation is investigated using the FE method then the analytical form (19) is not known. Suppose, we are given a strain loop in form of a sequence of discrete
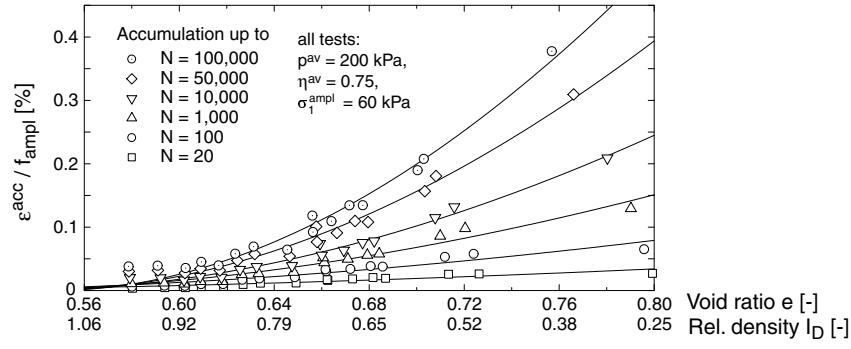
Figure 14: *Accumulated strain $\varepsilon^{\mathrm{acc}}$ in dependence on the actual void ratio e for different numbers of cycles. The $f_{\mathrm{ampl}}$-variability has been removed here.*

| Function | Mat. constants | | typical range of the function response | remarks |
|---|---|---|---|---|
| $f_{\mathrm{ampl}} = \left( \dfrac{\epsilon^{\mathrm{ampl}}}{\epsilon^{\mathrm{ampl}}_{\mathrm{ref}}} \right)^2$ or (9) | $\epsilon^{\mathrm{ampl}}_{\mathrm{ref}}$ | $10^{-4}$ | $0\ldots 100$ | |
| $\dot{f}_N = \dfrac{C_{N1} C_{N2}}{1 + C_{N2}\, N} + C_{N1} C_{N3}$ | $C_{N1}$ | $3.4 \cdot 10^{-4}$ | $(0.1\ldots 0.2)\,10^{-3}$ | $0 < N < \infty$ |
| | $C_{N2}$ | $0.55$ | | |
| | $C_{N3}$ | $6.0 \cdot 10^{-5}$ | | |
| $f_p = \exp\left[ -C_p \left( \dfrac{p^{\mathrm{av}}}{p_{\mathrm{atm}}} - 1 \right) \right]$ | $C_p$ | $0.43$ | $1.5\ldots 0.02$ | $50 \le p \le 300$ kPa |
| | $p_{\mathrm{atm}}$ | $100$ kPa | | |
| $f_Y = \exp\left( C_Y\, \bar{Y}^{\mathrm{av}} \right)$ | $C_Y$ | $2.0$ | $1\ldots 7.4$ | $0 < \bar{Y} < 1.1$ |
| $f_e = \dfrac{(C_e - e)^2}{1 + e} \dfrac{1 + e_{\mathrm{ref}}}{(C_e - e_{\mathrm{ref}})^2}$ | $C_e$ | $0.54$ | $1\ldots 0$ | |
| | $e_{\mathrm{ref}}$ | $0.874$ | | |
| $f_\pi = 1 + C_{\pi 1}\left[ 1 - \left( \overrightarrow{\mathbf{A}}_\varepsilon :: \boldsymbol{\pi} \right) \right]$ | $C_{\pi 1}$ | $4.0$ | $1\ldots 4$ | quickly declines |
| $\boldsymbol{\pi} + \Delta\boldsymbol{\pi} = \mathcal{R} : \boldsymbol{\pi}$ with (24) | $C_{\pi 2}$ | $200$ | | |

Table 1: *Summary of the partial functions $f_i$ and a list of the material constants $C_i$ for the tested sand.*

strains $\boldsymbol{\epsilon}(t_k)$, $k = 1, \ldots, M$ recorded by an FE program at a Gauss point. In order to formulate a suitable definition of the tensorial amplitude $\mathsf{A}_\epsilon$ we keep in mind the following observations:

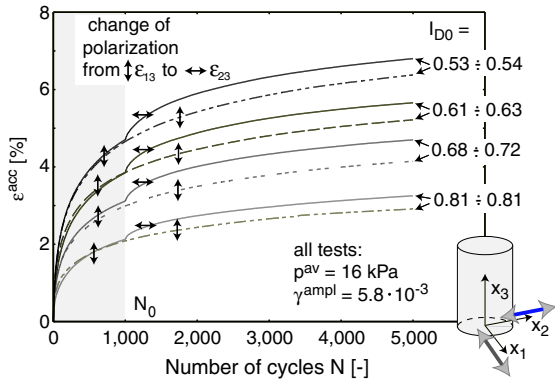- The shape of the strain cycle, Figure 16, influences the accumulation rate.



Figure 17: *After a sudden change of polarization $\vec{\mathsf{A}}_\epsilon$ the rate of accumulation leaps.*

- The orientation (= polarization) of the cycle in the strain space is of importance, Figure 17. A sudden change of the polarization may increase the rate of accumulation [2].

- The strain states upon a cycle need not be coaxial and therefore the paths $\boldsymbol{\epsilon}(t)$ are 6-dimensional.

- The size of the 6-dimensional strain path must be described by 6 extents (further called *spans*).

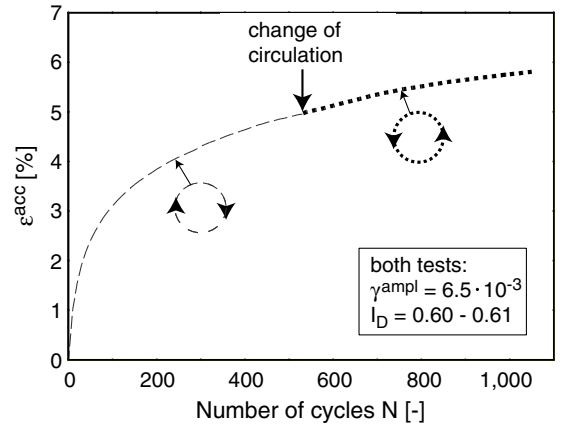- Polarization cannot have a sign, i.e. it has a direction but no *sense of the direction*.



Figure 18: *A change of the circulation of the cyclic strain path does not affect the accumulation.*

- A change of circulation has no effect. Figure 18 does not show any change of the accumulation rate after the circulation was changed from the clockwise ↻ to the counterclockwise ↺,

From a recorded cycle $\boldsymbol{\epsilon}(t_k)$ with $k = 1, \ldots, M$ we may determine the pair of the two most distant points, say $\boldsymbol{\epsilon}(t_a)$ and $\boldsymbol{\epsilon}(t_b)$. The span of the cycle is quantified by its size $2R^{(6)} = \|\boldsymbol{\epsilon}(t_a) - \boldsymbol{\epsilon}(t_b)\|$ and its orientation $\vec{\mathbf{r}}^{(6)} = (\boldsymbol{\epsilon}(t_a) - \boldsymbol{\epsilon}(t_b))^{\rightarrow}$. The upper index $\sqcup^{(i)}$ corresponds to the maximum possible number of dimensions of the loop, e.g. the original strain path (before flattening) can be at most six-dimensional, $\boldsymbol{\epsilon}^{(6)} = \boldsymbol{\epsilon}$. In order to find the second longest span the strain loop is *projected* onto the hyperplane perpendicular to $\vec{\mathbf{r}}^{(6)}$. It results in the flattened strain trajectory $\boldsymbol{\epsilon}^{(5)} = \boldsymbol{\epsilon}^{(6)} - \vec{\mathbf{r}}^{(6)} : \boldsymbol{\epsilon}^{(6)} \otimes \vec{\mathbf{r}}^{(6)}$ which has at most five dimensions. The span of the flattened trajectory can be determined analogously and described by $R^{(5)}$ and $\vec{\mathbf{r}}^{(5)}$. The flattened loop is subjected to the subsequent projection, this time along $\vec{\mathbf{r}}^{(5)}$, etc. Of course $R^{(6)} \geq R^{(5)} \geq \cdots \geq R^{(1)}$ holds. The tensorial amplitude $\mathsf{A}_\epsilon$ is proposed to be defined as the following sum

$$\mathsf{A}_\epsilon = \sum_{i=1}^{6} R^{(i)} \; \vec{\mathbf{r}}^{(i)} \otimes \vec{\mathbf{r}}^{(i)} . \tag{21}$$

collecting all spans[8]. Briefly speaking, the described method

**Projection of ε(t) from 3D to 2D**
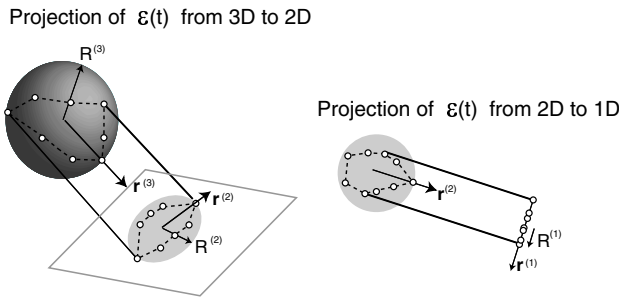


**Projection of ε(t) from 2D to 1D**

Figure 19: *The directions $\vec{r}_i$ and the sizes $R^{(i)}$ of the strain loop.*

consists in a gradual degeneration of the strain path in order to determine its spans. The sense of the direction of $\vec{\mathbf{r}}^{(i)}$ is of no importance, which is obvious from (21). For numerical efficiency the calculation can be aborted if the size of the subsequent span is negligible (say less than 10% of the largest span). Projections from a 3-dimensional path to the 1-dimensional path are shown in Figure 19.

From the above algorithm a list of radii $R^{(6)} \geq R^{(5)} \geq \cdots \geq R^{(1)}$ and a list of mutually orthogonal orientations: $\vec{\mathbf{r}}^{(6)}, \vec{\mathbf{r}}^{(5)}, \ldots, \vec{\mathbf{r}}^{(1)}$ are obtained[9]. Substituted into (21) they constitute the tensorial amplitude. The amplitude $\mathsf{A}_\epsilon$ is a 4-th order tensor which has the eigenvalues $R^{(i)}$ and the corresponding eigentensors $\vec{\mathbf{r}}^{(i)}$.

The normalized amplitude

$$\vec{\mathsf{A}}_\epsilon = \mathsf{A}_\epsilon / \|\mathsf{A}_\epsilon\| \tag{22}$$

is called *polarization* and the norm

$$\epsilon^{\mathrm{ampl}} = \|\mathsf{A}_\epsilon\| = \sqrt{\left(R^{(6)}\right)^2 + \left(R^{(5)}\right)^2 + \cdots + \left(R^{(1)}\right)^2} \tag{23}$$

---

[8]An analogous definition using the $\frac{1}{4}$-th of the perimeters $P^{(i)}$ of the loops instead of the radii $R^{(i)}$ lead to a worse approximation of the experiments.

[9]A fortran-90 implementation of the above algorithm is available from the first author.

is the scalar amplitude. For harmonic cycles of type (19), definition (23) simplifies to (20). This can be demonstrated with a simple MATHEMATICA script

```
degenerate[epsilon_]:=(* argument is a list of functions of t *)
  Module[
    {rr, solution, nmax, rrmax, tmax, polarization,R,degenerated},
    rr = epsilon.epsilon;
    solution = NSolve[Evaluate[D[rr, t] == 0], t];
    nmax = Length[solution];
    rrmax = Table[0, {nmax}];
    Do[rrmax[[i]]=Evaluate[rr/.solution[[i]]],{i,1,nmax}];
    tmax = t /. solution[[Ordering[rrmax][[nmax]]]];
    p = epsilon /. t -> tmax;
    polarization = p/Sqrt[p.p];
    R = Sqrt[ Max[rrmax] ];
    degenerated = epsilon-polarization*(epsilon.polarization);
    {R, polarization, degenerated}
  ]
example = {e1->3, e2->1, e3->2, th2->Pi/3.0, th3->Pi/6.0 };
epsilon3 = { e1 Sin[t], e2 Sin[t+th2], e3 Sin[t+th3]} /. example;
{R3, p3, epsilon2} = degenerate[epsilon3];
{R2, p2, epsilon1} = degenerate[epsilon2];
ParametricPlot3D[epsilon3, {t, 0, 2 Pi} ];
ParametricPlot3D[epsilon2, {t, 0, 2 Pi} ];
R3^2 + R2^2 == e1^2 + e2^2 + e3^2 /. example
```

## 3.2 Back polarization $\boldsymbol{\pi}$ and function $f_\pi$

If a package of cycles with the amplitude $\mathsf{A}_\epsilon^{(1)}$ is directly followed by another package with the amplitude $\mathsf{A}_\epsilon^{(2)}$ with the same polarization, i.e. $\vec{\mathsf{A}}_\epsilon^{(1)} :: \vec{\mathsf{A}}_\epsilon^{(2)} = 1$, no correction of the accumulation rate is needed ($f_\pi = 1$) except for $f_{\mathrm{ampl}}$. However, if the polarization has changed then the above product may become significantly smaller (in the extreme case $\vec{\mathsf{A}}_\epsilon^{(1)} :: \vec{\mathsf{A}}_\epsilon^{(2)} = 0$) and then the rate of accumulation is increased ($f_\pi > 1$), Figure 17. The function $f_\pi$ which enters (7) takes this effect into account.

Let us introduce the 4-th rank back polarization tensor $\boldsymbol{\pi}$ which represents the polarization in the recent history of cyclic deformation. The rate of accumulation is proposed to be a function of the angle $\alpha = \arccos(\vec{\mathsf{A}}_\epsilon :: \boldsymbol{\pi})$ between the current polarization $\vec{\mathsf{A}}_\epsilon$ and $\boldsymbol{\pi}$, Figure 20.

The product $0 \leq \boldsymbol{\pi} :: \vec{\mathsf{A}}_\epsilon \leq 1$ reflects the degree of adaptation of the soil structure to the current polarization. During cycles with $\vec{\mathsf{A}}_\epsilon = $ const the tensor $\boldsymbol{\pi}$ is evolving, asymptotically approaching the current polarization, $\boldsymbol{\pi} \to \vec{\mathsf{A}}_\epsilon$. Since both $\boldsymbol{\pi}$ and $\vec{\mathsf{A}}_\epsilon$ are unit tensors the evolution of $\boldsymbol{\pi}$ is a kind of *rotation* diminishing the angle $\alpha$, Figure 20.

The angle $\alpha$ is proposed to evolve according to

$$\dot{\alpha} = -C_{\pi 2} \; \alpha \; (\epsilon^{\mathrm{ampl}})^2 \tag{24}$$

meaning that the rate of change of $\alpha$ is proportional to $-\alpha$ and to the square of the amplitude. The constant $C_{\pi 2}$ is positive so the back polarization indeed tends towards the current polarization, $\boldsymbol{\pi} \to \vec{\mathsf{A}}_\epsilon$. In order to update $\boldsymbol{\pi}$ we rotate it,

$$\boldsymbol{\pi} + \Delta\boldsymbol{\pi} = \mathcal{R} :: \boldsymbol{\pi}, \tag{25}$$

by the angle $\Delta\alpha = \dot{\alpha}\Delta N$, wherein the rotation operator is defined by

$$\mathcal{R} = (\cos\Delta\alpha - 1)(\vec{\boldsymbol{\mu}} \otimes \vec{\boldsymbol{\mu}} + \vec{\boldsymbol{\nu}} \otimes \vec{\boldsymbol{\nu}}) + \sin\Delta\alpha(\vec{\boldsymbol{\nu}} \otimes \vec{\boldsymbol{\mu}} - \vec{\boldsymbol{\mu}} \otimes \vec{\boldsymbol{\nu}}) + \mathsf{J} \tag{26}$$

and where $\boldsymbol{\mu} = \vec{\mathsf{A}}_\epsilon + \boldsymbol{\pi}$ and $\boldsymbol{\nu} = \vec{\mathsf{A}}_\epsilon - \boldsymbol{\pi}$ denote mutually orthogonal tensors constructed on the hyperplane perpendicular to the rotation axis. $\mathsf{J}$ denotes the 8-th rank identity tensor.
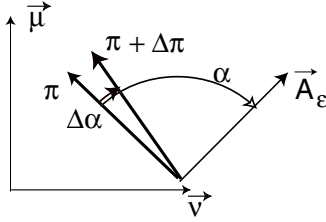
Figure 20: *Evolution of $\boldsymbol{\pi}$ can be seen as a rotation in 6-D space.*

An increase in the rate of accumulation can be described by the factor

$$f_\pi = 1 + C_{\pi 1}\left(1 - \cos\alpha\right). \tag{27}$$

The material constants $C_{\pi 1}$ and $C_{\pi 2}$ can be determined from an increased accumulation rate due to a rapid change of polarization, Figure 17. The presented tests have been carried out in our multiaxial direct simple shear (DSS) device. Its novelty lies in a possibility of the lower end plate to move (cyclically) along an arbitrary horizontal trajectory, [2].

Let us begin a DSS test applying a large number of $\epsilon_{13}$-cycles, Figure 17. At first the back polarization tensor $\boldsymbol{\pi}$ is undetermined but according to (24) it must tend asymptotically (with $N$) to the stationary value $\boldsymbol{\pi} = \vec{A}_\epsilon$ corresponding to $f_\pi \approx 1$. After several hundred cycles $\boldsymbol{\pi}$ may be expected to have reached this asymptotic value. Then the polarization $\vec{A}_\epsilon$ of the applied loading is rapidly rotated, whereas $\boldsymbol{\pi}$ is left unchanged. In Figure 17 the $\epsilon_{13}$-shearing is followed by the orthogonally polarized $\epsilon_{23}$-shearing. This change of polarization corresponds to $\alpha = 90°$. According to (27) the rate of accumulation of the axial strain recorded during the test must increase $f_\pi = (1 + C_{\pi 1})$-times with respect to the rate of accumulation under the previous $\epsilon_{13}$-cycles. Knowing this increase one can determine $C_{\pi 1}$. Further, it can be seen from Figure 17 that the additional rate of accumulation declines with $N$ vanishing completely after several hundred cycles. The solid curve corresponding to $\epsilon_{23}$-cycles becomes parallel to the dashed curve of $\epsilon_{13}$-cycles. The constant $C_{\pi 2}$ can be found fitting the measured curve $f_\pi(N)$ with $f_\pi(N) = 1 + C_{\pi 1}\left[1 - \cos\left(\alpha_0 \exp\left[-C_{\pi 2}(\epsilon^{\mathrm{ampl}})^2(N - N_0)\right]\right)\right]$ for $N \geq N_0$, wherein $N_0$ is the number of cycles prior to the rapid change of polarization. This formula can be easily derived integrating $\dot\alpha$ from (24) with respect to $N$ and substituting the result (i.e. $\alpha$) into (27).

For in-situ soils subjected to a vertical cyclic preloading $\boldsymbol{\pi}$ may be initiated with

$$\boldsymbol{\pi} = \vec{A}_\epsilon = \vec{r} \otimes \vec{r}, \tag{28}$$

wherein $\vec{r}$ corresponds to the vertical compression. The spectrum of $\boldsymbol{\pi}$ is $\{0, 0, 0, 0, 0, 0, 0, 0, 1\}$ and the non-zero eigenvalue corresponds to the prescribed eigenvector $\vec{r}$. Another extreme example could be a fresh sand fill with a perfectly *isotropic* structure, i.e. with no privileged direction of cyclic strain. The corresponding back polarization

$$\boldsymbol{\pi}^{\mathrm{iso}} = \frac{1}{3}\mathsf{J} \tag{29}$$

can be obtained integrating the dyadic product $\vec{r} \otimes \vec{r}$ over all directions in the strain space and dividing the result by the surface of the 6-dimensional hypersphere.

## 3.3 Interference of amplitudes from several excitation sources

Suppose we have two sources, (1) and (2), of cyclic loading *simultaneously* causing deformations at a point of interest. Since the sizes, frequencies and polarizations of the strain loops from the individual sources may be quite different the resulting strain path may be very complicated. Due to the quadratic dependence of the accumulation rate on the strain amplitude, $\|\mathbf{D}^{\mathrm{acc}}\| \sim (\epsilon^{\mathrm{ampl}})^2$, described by the function $f_{\mathrm{ampl}}$ the superposition

$$f_{\mathrm{ampl}}(\mathsf{A}_\epsilon^{(1+2)}) \stackrel{?}{=} f_{\mathrm{ampl}}(\mathsf{A}_\epsilon^{(1)}) + f_{\mathrm{ampl}}(\mathsf{A}_\epsilon^{(2)}), \tag{30}$$

of the accumulation rates is not evident, unless the amplitudes are mutually orthogonal and of harmonic type as defined in (19). With $\mathsf{A}_\epsilon^{(1)} :: \mathsf{A}_\epsilon^{(2)} = 0$ and with identical frequencies, $\nu^{(1)} = \nu^{(2)}$ the accumulation rate is proportional to

$$\left\|\mathsf{A}_\epsilon^{(1)} + \mathsf{A}_\epsilon^{(2)}\right\|^2 = \left\|\mathsf{A}_\epsilon^{(1)}\right\|^2 + \left\|\mathsf{A}_\epsilon^{(2)}\right\|^2. \tag{31}$$

Hence, the accumulations from orthogonal harmonic cycles are additive.

Another special case is the interference of two harmonic oscillations of the same frequency and proportional amplitudes $\mathsf{A}_\epsilon^{(2)} = \lambda\mathsf{A}_\epsilon^{(1)}$. The accumulation rate is proportional to $\left(\epsilon^{\mathrm{ampl}\ (1+2)}\right)^2 = (1 + \lambda^2 + 2\lambda\cos\Delta\theta)\left\|\mathsf{A}_\epsilon^{(1)}\right\|^2$ wherein $\Delta\theta$ is the phase difference between the signals and $2\lambda\cos\Delta\theta$ denotes the *interference effect*. For the sake of simplicity, we assume further $2\lambda\cos\Delta\theta = 2\lambda$ which may lead to overestimations of the accumulation rate. In the following the above special cases will be generalized.

In 1-D fatigue models the peaks of the strain path $\epsilon(t)$ are often paired into so-called rainflow cycles, each consisting of a local minimum and a maximum. The pairs are counted and substituted into (12) according to their size. For $n$-dimensional problems an analogous method of the separation of cycles is known as multiaxial rainflow counting. The peaks are detected by the unloading criterion using a construction similar to the one of the 'multi-surface plasticity'. The size of a sub-cycle is defined to be the diameter of the corresponding subsurface. We have not decided to use this method for two reasons. Firstly, a large common multiple of the frequencies $\nu^{(1)}$ and $\nu^{(2)}$ may render the repeatable sequence of loading very long. Secondly, the multiaxial rainflow counting can be excessively sensitive to small changes in the input strain path. For example, Figure 21, if one slightly modified a circular strain cycle forming a shallow (but long) concavity then such unloading could be interpreted as an additional sub-cycle of a considerable size.
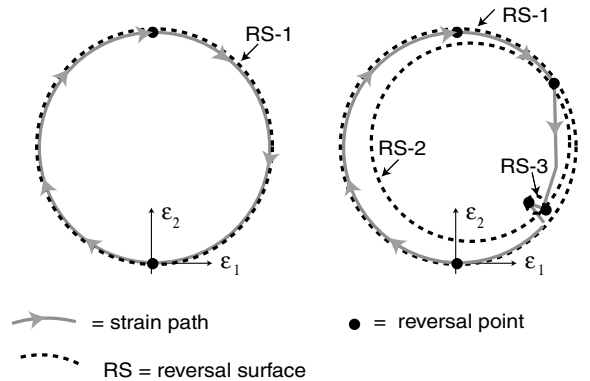


Figure 21: *A multiaxial rainflow counting algorithm has a shortcoming: a relatively small modification of the strain path generates the reversal surface RS-2 of a considerable size. RS-2 is counted as a sub-cycle.*

Dealing with interferences of cycles from several $(i = 1, \ldots, m)$ sources of the same frequency we propose just to add all amplitudes. In order to explain this approximation let us consider two oscillations with identical frequency $\nu^{(1)} = \nu^{(2)}$ but

different amplitudes $A_\epsilon^{(1)} \neq A_\epsilon^{(2)}$. Let $A_\epsilon^{(1)}$ denote (by convention) the dominating amplitude, i.e. $\epsilon^{\text{ampl (1)}} > \epsilon^{\text{ampl (2)}}$. It is legitimate to decompose the second amplitude $A_\epsilon^{(2)}$ into two orthogonal parts

$$A_\epsilon^{(2)} = A_\epsilon^{(2)\parallel} + A_\epsilon^{(2)\perp}, \tag{32}$$

wherein the part $A_\epsilon^{(2)\parallel}$ is parallel to $A_\epsilon^{(1)}$. It can be found by the projection of $A_\epsilon^{(2)}$ onto the direction of the dominant amplitude $A_\epsilon^{(1)}$, viz.

$$A_\epsilon^{(2)\parallel} = (\vec{A}_\epsilon^{(1)} :: A_\epsilon^{(2)})\vec{A}_\epsilon^{(1)} = \lambda A_\epsilon^{(1)} \tag{33}$$

As already mentioned, accumulation rates due to orthogonal amplitudes $A_\epsilon^{(2)\perp}$ and $A_\epsilon^{(1)}$ are additive. Now, let us examine the square of the Euclidean norm of the sum of the amplitudes

$$\left\| A_\epsilon^{(1)} + A_\epsilon^{(2)} \right\|^2 = \left\| (1+\lambda)A_\epsilon^{(1)} + A_\epsilon^{(2)\perp} \right\|^2 =$$
$$(1+\lambda)^2 \left\| A_\epsilon^{(1)} \right\|^2 + \left\| A_\epsilon^{(2)\perp} \right\|^2 \tag{34}$$

In order to estimate the joint contribution from several oscillations we may just add (component-wise) their amplitudes. This "approximate" superposition requires the aforementioned assumption $2\lambda \cos \Delta\theta \approx 2\lambda$ pertaining to the phase shift.

If the interfering oscillations have different frequencies then the correction factor $\sqrt{\nu_i/\nu_1}$ should be applied. Hence, the final expression has the form

$$A_\epsilon = \sum_{i=1}^{m} \sqrt{\frac{\nu_i}{\nu_1}} A_\epsilon^{(i)}. \tag{35}$$

The number of cycles (variable $N$) is common for all oscillations and it is dictated by the frequency $\nu^{(1)}$ of the dominant cyclic loading. Correction (35) is not strict. This approximation has been derived using an older explicit model [20] based on the approximation $\dot{f}_N f_{\text{ampl}} = C_{N1}C_{N2}/(1+C_{N2}\tilde{N})$ with $\tilde{N} = \left(\epsilon^{\text{ampl}}\right)^2 N$.

# 4   FE implementation

The presented model has been implemented as a user's material model (= fortran routine umat) into the commercial FE program ABAQUS [42]. ABAQUS uses the implicit time integration and the full Newton solution technique. The purpose of umat is to update the stress and all user-defined state variables basing on their current values and on the strain increment. Moreover umat should return the tangential constitutive stiffness (Jacobian matrix) because the total stiffness matrix is recalculated in every iteration (full Newton). The strain increment is being improved in the course of the equilibrium iteration. During this iteration umat obtains the state variables relevant to the beginning of the increment, i.e., no partial updates are performed during the iterations. This is advantageous in particular for cyclic problems because no artificial (numerical) unloadings are possible within a single increment.

The fortran subroutine umat has three modes of operation:

1. *Implicit mode*: umat delegates the calculation to the 'implicit umat' treated as a subordinated procedure. As the 'implicit umat' we use a version of the hypoplastic constitutive model with the so-called intergranular strain (cf. [28] and [3] Sections 2.5, 4.1 and 4.3.6) The material constants used in calculations are listed in Table 3. The implicit mode is used to find the initial state equilibrium and to perform irregular cycles. The numerical implementation of hypoplasticity is discussed in [3] in Section 4.1.3.

2. *Recording mode*: umat works in the implicit mode (hypoplasticity) but additionally the strain path is memorized. Only a few characteristic states need to be recorded. Several filtering criteria have been devised to economise on the computer memory. The recording mode provides the input data for the calculation of the field of strain amplitudes.

3. *Pseudo-creep mode*: umat calculates stress increments explicitly using (5) and (7). Before the first increment is executed in this mode, the amplitude $A_\epsilon$ is evaluated.

The subroutine umat can recognize the modes of operation by the number of the step[10].

The recording of the strain path is schematically illustrated in Figure 22. Only several strain states (marked with filled circles) are recorded, namely the first one and those which satisfy the condition

$$\cos \beta = \vec{\epsilon}_R : \vec{\Delta\epsilon} > 0.9 \quad \text{and} \quad \|\epsilon_R\| > 10^{-5}, \tag{36}$$

wherein $\epsilon_R$ is measured from the recently recorded strain and $\Delta\epsilon$ denotes the current strain increment, Figure 22. Full tensors $\epsilon(t_k)$ must be recorded because they can be non-coaxial.

The explicit calculations are mesh-size dependent if the accumulated strain (in particular the function $f_{\text{ampl}}$) is assumed constant over an element. It is recommended [43, 44] to choose elements with quadratic shape functions. Compared to the viscoplasticity, the accumulation rate $\mathbf{D}^{\text{acc}}$ is not very sensitive to changes in stress and void ratio. Since the numerical convergence does not pose serious problems in the FE implementation, a simplified tangential stiffness is used. In particular, the terms $(\partial \mathbf{D}^{\text{acc}}/\partial \mathbf{T}) : (\partial \mathbf{T}/\partial \mathbf{D})$ and $(\partial \mathbf{D}^{\text{acc}}/\partial e)(\partial e/\partial \mathbf{D})$ are negligible compared to $(\partial \mathring{\mathbf{T}}/\partial \mathbf{D})$ and hence disregarded. If the loading criterion (6) is satisfied the elastoplastic stiffness $\mathsf{E}^{\text{ep}}$ instead of $\mathsf{E}$ enters the Jacobian matrix. In the pseudo-creep phase we use

$$\Delta g^A = f_{\text{ampl}} C_{N1} \ln \left[ 1 + C_{N2}\Delta N \exp \left( \frac{-g^A}{f_{\text{ampl}}C_{N1}} \right) \right] \tag{37}$$

in place of $\dot{g}^A \Delta N$ given by the first term of (14). This enhances the accuracy of the calculation for large increments $\Delta N$. The pseudo-creep mode can be seen as an initial strain problem consisting in the determination of the displacement field from a given strain field. Integration of the prescribed strains into displacements may generate self-stresses. The self-stresses of physical origin are caused by the incompatibilities of the strain field

$$e_{imk}e_{jnl}\epsilon_{kl,mn} \neq 0_{ij}. \tag{38}$$

This expression simplifies to $\epsilon_{11,22}^{\text{acc}} + \epsilon_{22,11}^{\text{acc}} - 2\epsilon_{12,12}^{\text{acc}} \neq 0$ for plane strain problems. Considerable "artificial" self-stresses may be caused by the FE solution method (a problem analogous to locking). If poor shape functions are used, the prescribed strains cannot be matched to the nodal displacements. In order to alleviate this problem we use 8-nodal plane strain elements with reduced integration [45].

# 5   Example of FE-calculation

The proposed material model has been used to simulate a centrifuge model test (under increased gravity of $20g$), Figure 23. In this test [46] a strip foundation (with a prototype width $b = 1$ m) was placed without embedment on a freshly pluviated dense fine sand ($\varrho_s = 2{,}66$ g/cm$^3$, $e_{\min} = 0.575$, $e_{\max} = 0.908$, $d_{50} = 0.21$ mm, $U = d_{60}/d_{10} = 1.95$, $I_D \approx 0.90$) and cyclically loaded between 4 % and 47 % of the static bearing capacity of 345 kN. The vertical load was chosen as $Q^{\text{av}} = 88.7$
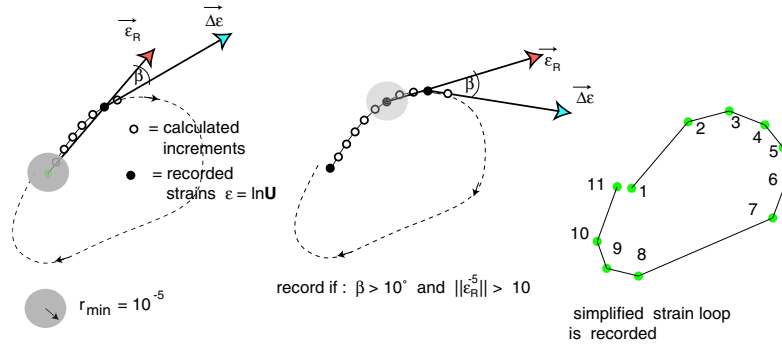
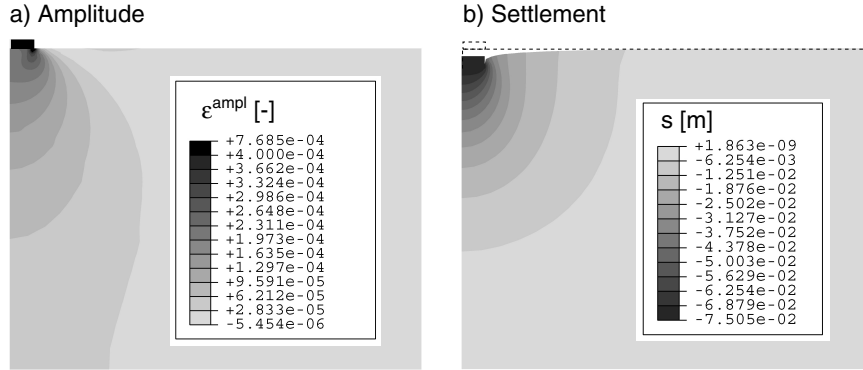Figure 22: *Recording of strain states along the loop.*



Figure 25: *a) Field of strain amplitude $\varepsilon^{\mathrm{ampl}}$, b) Field of accumulated settlement $s^{\mathrm{acc}}$ after $N = 100{,}000$ cycles*
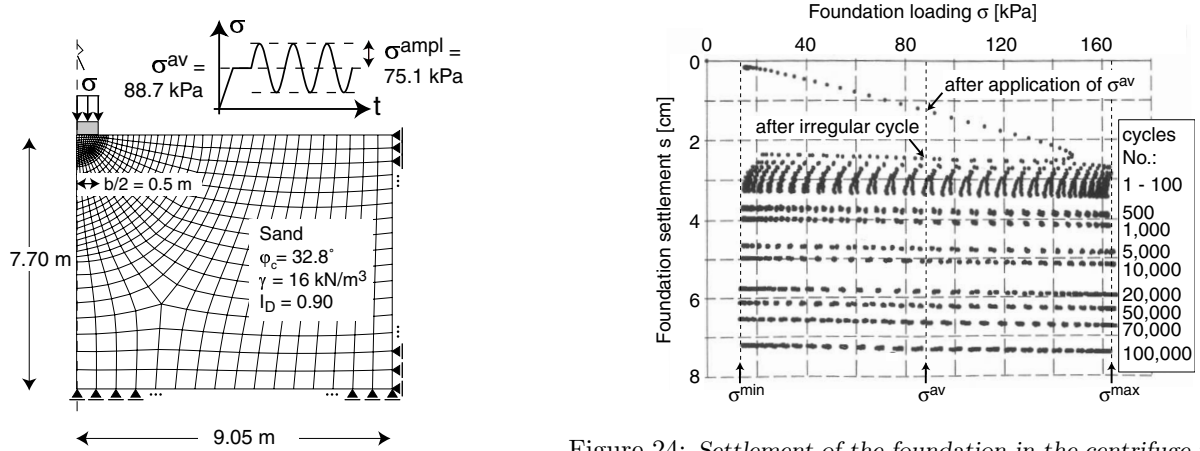


Figure 23: *Geometry of the prototype and soil parameters of the centrifuge test.*



Figure 24: *Settlement of the foundation in the centrifuge test as a function of the number of cycles.*

kN, $Q^{\mathrm{ampl}} = 75.1$ kN and the frequency was 0.44 Hz. Several load-settlement curves generated by the cycles 1-100, as well as the cycle 500, ... are plotted in Figure 24 (prototype scale). The vertical displacement amplitude was $s^{\mathrm{ampl}} = 0.8$ mm and the accumulated settlement after $N = 10^5$ cycles was $s = 7.3$ cm.

The sand used in the centrifuge test was similar (but not identical) to the laboratory sand described in this paper. Therefore several material constants $C_{N1} = 1.21 \cdot 10^{-3}$, $C_{N2} = 0.39$, $C_{N3} = 5.7 \cdot 10^{-5}$, $C_e = 0.52$ and $e_{\mathrm{ref}} = 0.908$ have been determined in additional tests. The remaining constants are assumed equal to the ones of the laboratory sand, see Table

2. The hypoplasticity constants in Table 3 have been determined from standard laboratory tests except for $m_T$, $m_R$ and $\beta_R$ which had been taken from the literature [3,28,47] and then slightly adjusted to improve the simulation of the second cycle of the centrifuge test (estimation of amplitude).

The FE-calculation was commenced from the geostatic stress with $K_0 = 0.43$. The initial cyclic history has been assumed $g^A = 0$ because the centrifuge test was performed on freshly pluviated sand. Only a half of the $18.10 \times 7.70$ m subsoil (prototype dimensions) has been discretized taking advantage of the symmetry. Quadrilateral 8-nodal elements have been used with reduced integration and an hourglass mode control.

Figure 25a presents the resulting field of the strain amplitude $\varepsilon^{\mathrm{ampl}}$. The field of the numerically obtained settlements $s$ after 100,000 cycles is presented in Figure 25b, in particular the settlement of the foundation is $s = 7.5$ cm. The calculated

---

[10]ABAQUS applies loads via steps. Each step may consist of many increments and each increment may need many equilibrium iterations.

13

| $\varepsilon_{\text{ref}}^{\text{ampl}}$ [−] | $C_{N1}$ [-] | $C_{N2}$ [-] | $C_{N3}$ [-] | $C_p$ [-] | $p_{\text{ref}}$ [kPa] | $C_Y$ [-] | $C_e$ [-] | $e_{\text{ref}}$ [-] |
|---|---|---|---|---|---|---|---|---|
| $10^{-4}$ | $1.21 \cdot 10^{-3}$ | 0.39 | $5.7 \cdot 10^{-5}$ | 0.43 | 100 | 2.0 | 0.52 | 0.908 |

Table 2: *Constants of the accumulation model for the 'centrifuge sand'.*

| $\varphi_c$ [°] | $h_s$ [MPa] | $\nu$ [-] | $n$ [-] | $e_{d0}$ [-] | $e_{c0}$ [-] | $e_{i0}$ [-] | $\alpha$ [-] | $\beta$ [-] | $R$ [-] | $m_R$ [-] | $m_T$ [-] | $\chi$ [-] | $\beta_R$ [-] |
|---|---|---|---|---|---|---|---|---|---|---|---|---|---|
| 32.8 | 150 | 0.2 | 0.40 | 0.575 | 0.908 | 1.044 | 0.12 | 1.0 | $10^{-4}$ | 6.5 | 3 | 6 | 0.1 |

Table 3: *Constants of the hypoplastic model used in the implicit steps*

settlement $s(N)$ is compared to the measured test values in Figure 26. The calculated and measured curves are in a fairly
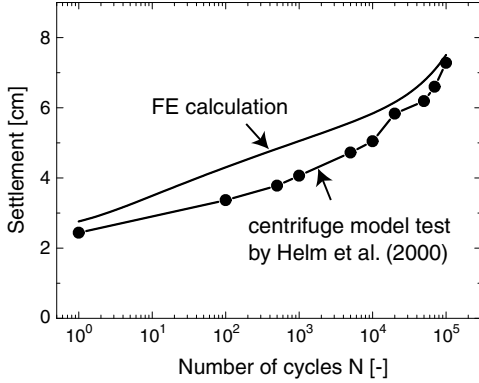


Figure 26: *Accumulation of foundation settlement during the regular cycles: FE calculation versus model test.*

good agreement At the beginning of the simulation some discrepancy between measured and calculated data was caused by an inaccurate prediction of the residual settlement after the irregular cycle. Discussion of this discrepancy is irrelevant in this paper because the implicit model is responsible for it.

The numerical performance of the presented model is satisfactory. The mesh dependence becomes noticeable only for relative coarse discretizations (less than 100 elements). Only sporadically some unexplained convergence problems appear in the *implicit* mode if ABAQUS contact elements were used. In order to allow for the automatic time incrementation the number of cycles $N$ has been set to be identical to the 'steptime' in the *pseudo creep* mode. It is recommended to begin calculations in the *pseudo creep* mode from a small increment (we have started with $\Delta N = 0.01$). The time step is promptly increased to $\Delta N = 500$ cycles or more.

# 6 ACKNOWLEDGEMENTS

# 7 APPENDIX A

Vectors and tensors are distinguished by bold typeface, for example $\mathbf{T}, \mathbf{v}$ or in sans serif font (e.g. E). The symbol $\cdot$ denotes multiplication with one dummy index (single contraction), e.g. the scalar product of two vectors can be written as $\mathbf{a} \cdot \mathbf{b} = a_k b_k$. Multiplication with two dummy indices (double contraction) is denoted with a colon, e.g. $\mathbf{A} : \mathbf{B} = \text{tr}(\mathbf{A} \cdot \mathbf{B}^T) = A_{ij}B_{ij}$, wherein $\text{tr}\,\mathbf{X} = X_{kk}$ reads trace of a tensor. The superscript $\sqcup^T$ denotes transposition. Analogously we may define double colon :: to quadruple contraction with four dummy indices. Two fourth order identity tensors with symmetrization $I_{ijkl} = \frac{1}{2}(\delta_{ik}\delta_{jl} + \delta_{il}\delta_{jk})$ and without symmetrization $J_{ijkl} = \delta_{ik}\delta_{jl}$ are used. The brackets $\| \ \|$ denote the Euclidean norm. The deviatoric part of a tensor is denoted by an asterisk, e.g. $\mathbf{T}^* = \mathbf{T} - \frac{1}{3}\mathbf{1}\text{tr}\,\mathbf{T}$, wherein $(\mathbf{1})_{ij} = \delta_{ij}$ stands for the Kronecker's symbol. The operator $(\ )_{ij}$ extracts the $ij$-th component from the tensor in brackets. Permutation symbol is denoted by $e_{ijk}$. Dyadic multiplication is written with $\otimes$, e.g. $(\mathbf{a} \otimes \mathbf{b})_{ij} = a_i b_j$ or $(\mathbf{T} \otimes \mathbf{1})_{ijkl} = T_{ij}\delta_{kl}$. Positively proportional quantities are denoted by a tilde, e.g. $\mathbf{T} \sim \mathbf{D}$. Normalized quantities are denoted by an arrow and tensors divided by their traces are denoted with a hat, for example $\vec{\mathbf{D}} = \mathbf{D}/\|\mathbf{D}\|$ and $\hat{\mathbf{T}} = \mathbf{T}/\text{tr}\,\mathbf{T}$. The sign convention of general mechanics with *tension positive* is obeyed. The superposed dot, $\sqcup$, denotes the material rate (with respect to $N$) and the superposed circle $\sqcup$ denotes the Zaremba-Jaumann rate (finite rotations are accounted for).

The effective Cauchy stress $\mathbf{T}$, the stretching $\mathbf{D}$ and the total deformation is expressed by the logarithmic strain $\boldsymbol{\epsilon} = \ln \mathbf{U}$ is used throughout the text ($\mathbf{U}$ denotes the right stretch tensor). Generally, it would be inaccurate to interpret $\mathbf{D}$ as a time derivative of the strain $\boldsymbol{\epsilon}$ given by (4). In the axisymmetric case, alternatively to the popular Roscoe's variables:

$$p = -(T_1 + T_2 + T_3)/3; \quad q = -T_1 + (T_2 + T_3)/2 \quad (39)$$

$$\epsilon_v = -(\epsilon_1 + \epsilon_2 + \epsilon_3); \quad \epsilon_q = -\frac{2}{3}(\epsilon_1 - \frac{1}{2}(\epsilon_2 + \epsilon_3)) \quad (40)$$

$$D_v = -(D_1 + D_2 + D_3); \quad D_q = -(2D_1 - D_2 - D_3)/3 \quad (41)$$

the 'normalized', or isomorphic [3], variables :

$$P = \sqrt{3}p, \quad Q = \sqrt{\frac{2}{3}}q, \quad (42)$$

$$\epsilon_P = \frac{1}{\sqrt{3}}\epsilon_v \quad \epsilon_Q = \sqrt{\frac{3}{2}}\epsilon_q \quad (43)$$

$$D_P = \frac{1}{\sqrt{3}}D_v \quad D_Q = \sqrt{\frac{3}{2}}D_q \quad (44)$$

are used. The isomorphic variables preserve orthogonality and distance. Note that $P^2 = \|\frac{1}{3}\mathbf{1}\text{tr}\,\mathbf{T}\|^2$; $Q^2 = \|\mathbf{T}^*\|^2$ and $D_P^2 = \|\frac{1}{3}\mathbf{1}\text{tr}\,\mathbf{D}\|^2$; $D_Q^2 = \|\mathbf{D}^*\|^2$ hold. In the 6-D space the isomorphic components of strain are
$\{\epsilon_{11}, \epsilon_{22}, \epsilon_{33}, \sqrt{2}\epsilon_{12}, \sqrt{2}\epsilon_{13}, \sqrt{2}\epsilon_{23}\}$ and
$\{T_{11}, T_{22}, T_{33}, \sqrt{2}T_{12}, \sqrt{2}T_{13}, \sqrt{2}T_{23}\}$.
The Matsuoka-Nakai [27] inequality $-I_1 I_2 / I_3 - (9 - \sin^2 \varphi_c)/(1-$

$\sin^2 \varphi_c) \leq 0$ with the critical friction angle $\varphi_c$ is used throughout this paper as the yield criterion. It is formulated using the basic invariants of the stress tensor: $I_1 = \text{tr } \mathbf{T}$, $I_2 = [\mathbf{T} : \mathbf{T} - (\text{tr } \mathbf{T})^2]/2$ and $I_3 = \det \mathbf{T}$.

# 8    APPENDIX B

Working with a typical settlement formula

$$s(N) = s_1 f(N) \tag{45}$$

one assumes that the information about the cyclic history can be obtained from the residual settlement after a single cycle, usually from $s_1$ after the first one. The derivative of $s(N)$ with respect to $N$ describes the settlement per cycle, e.g. the settlement due to the $K$-th cycle is

$$s_K = \left. \frac{\mathrm{d}s(N)}{\mathrm{d}N} \right|_{N=K} = s_1 f'(K) \tag{46}$$

Of course, in order to be objective, the predicted settlement due to a given cycle should not depend on how we count cycles (i.e., which cycle we call "the first"). Therefore, beside fitting the experimental observation, the function $f(N)$ must satisfy the objectivity criterion:

$$s'(N) = s_1 f'(N) = s_M f'(N - M) \tag{47}$$

in which $s_M$ is the settlement due to an arbitrarily chosen cycle No. $M$ (because someone may consider $M$ as the 'first' cycle). Substituting $s_M$ from (46) into (47) the objectivity condition takes the form

$$f'(N) \equiv f'(M)f'(N - M) \tag{48}$$

it can be shown that the widely used functions $f(N) = N^C$ or $f(N) = 1 + C \log(N)$, cf. [6,7], do not satisfy this condition. An objective (consistent) settlement formula is

$$s(N) = s_1 \frac{1}{C} \left[ 1 - \exp(-CN) \right] \tag{49}$$

wherein $C$ is a positive material constant. Indeed, one can conclude from (48) that $f'(N)$ has the form

$$f'(N) = \exp(-CN). \tag{50}$$

After integration of $f'(N)$ with respect to $N$ with the initial condition $f(0) = 0$ we arrive at (49).

# References

1. Wichtmann T, Niemunis A, Triantafyllidis T. Strain accumulation in sand due to drained uniaxial cyclic loading. In: Triantafyllidis T, editor, Cyclic Behaviour of Soils and Liquefaction Phenomena. Balkema, 2004; pp. 233–246. International Conference in Bochum, 31 March - 02 April 2004.

2. Wichtmann T, Niemunis A, Triantafyllidis T. The effect of volumetric and out-of-phase cyclic loading on strain accumulation. In: Triantafyllidis T, editor, Cyclic Behaviour of Soils and Liquefaction Phenomena. Balkema, 2004; pp. 247–256. International Conference in Bochum, 31 March - 02 April 2004.

3. Niemunis A. Extended hypoplastic models for soils. Ruhr-University Bochum, Institute of Soil Mechanics and Foundation Engineering, 2003. 34, available from www.pg.gda.pl/~aniem/an-liter.html.

4. Ekberg A. Rolling contact fatigue of railway wheels. Ph.D. thesis, Chalmers University of Technology, 2000. Solid Mechanics.

5. Papadopoulos IV. A new criterion of fatigue strength for out-of-phase bending and torsion of hard metals. International Journal of Fatigue 1994;16:377–384.

6. Hettler A. Verschiebungen starrer und elastischer Gründungskörper in Sand bei monotoner und zyklischer Belastung. Ph.D. thesis, Institut für Boden- und Felsmechanik der Universität Karlsruhe, 1981. Heft Nr. 90.

7. O'Riordan NJ. Effects of cyclic loading on the long term settlements of structures. In: O'Reilly M, Brown S, editors, Cyclic Loading of Soils. Blackie Glasgow, 1992; pp. 411–433.

8. Valanis KC, Lee CF. Endochronic theory of cyclic plasticity with applications. Journal of Applied Mechanics 1984; 51:367–374.

9. Chaboche JL. Constitutive equations for cyclic plasticity and cyclic viscoplasticity. International Journal of Plasticity 1989;5:247–302.

10. Chaboche JL. Modelling of ratchetting: evaluation of various approaches. European Journal of Mechanics 1994; 13(4):501–781.

11. Mróz Z, Norris VA, Zienkiewicz OC. An anisotropic hardening model for soils and its application to cyclic loading. International Journal for Numerical and Analytical Methods in Geomechanics 1978;2:203–221.

12. Barksdale RD. Laboratory evaluation of rutting in base course materials. In: Third International Conference on Structural Design of Asphalt Pavements. volume 3, 1972; pp. 161–174.

13. Lentz RW, Baladi GY. Constitutive equation for permanent strain of sand subjected to cyclic loading. In: Transportation Research Record. volume 810, 1981; pp. 50–54.

14. Khedr S. Deformation characteristics of granular base course in flexible pavements. In: Transportation Research Record. volume 1043, 1985; pp. 131–138.

15. Paute JL, Jouve P, Ragneau E. Modéle de calcul pour le dimensionnement des chaussées souples. Bulletin de Liaison des Laboratoires des Ponts et Chaussées 1988;156:21–36.

16. Hornych P, Corte JF, Paute JL. Étude des déformations permanentes sous chargements répétés de trois graves non traitées. Bulletin de Liaison des Laboratoires des Ponts et Chaussées 1993;184:77–84.

17. Sweere GTH. Unbound granular bases for roads. Ph.D. thesis, Delft University of Technology, Netherlands, 1990.

18. Wolff H, Visser AT. Incorporating elasto-plasticity in granular layer pavement design. In: Proceedings of Institution of Civil Engineers Transport. volume 105, 1994; pp. 259–272.

19. Vuong B. Evaluation of back-calculation and performance models using a full scale granular pavement tested with the accelerated loading facility (alf). In: Proceedings 4 th International Conference on the Bearing Capacity of Roads and Airfields, Minneapolis. 1994; pp. 183–197.

20. Sawicki A. An engineering model for compaction of sand under cyclic loading. Engineering Transactions 1987; 35:677–693.

21. Martin GR, Finn WDL, Seed HB. Fundamentals of liquefaction under cyclic loading. Journal of the Geotechnical Engineering Division ASCE 1975;101(GT5):423–439.

22. Bouckovalas G, Whitman RV, Marr WA. Permanent displacement of sand with cyclic loading. Journal of Geotechnical Engineering 1984;110(11):1606–1623.

23. Marr WA, Christian JT. Permanent displacements due to cyclic wave loading. Journal of the Geotechnical Engineering Division ASCE 1981;107(GT8):1129–1149.

24. Suiker ASJ. Fatigue behaviour of granular materials. Technical Report 7-98-119-3, Delft University of Technology, Faculty of Civil Engineering, 1998.

25. Suiker ASJ. Static and cyclic loading experiments on noncohesive granular materials. Technical Report 1-99-DUT-1, Delft University of Technology, Faculty of Civil Engineering, 1999.

26. Gotschol A. Veränderlich elastisches und plastisches Verhalten nichtbindiger Böden und Schotter unter zyklischdynamischer Beanspruchung. Ph.D. thesis, Universität Gh Kassel, 2002.

27. Matsuoka H, Nakai T. A new failure for soils in three-dimensional stresses. In: Deformation and Failure of Granular Materials. 1982; pp. 253–263. Proc. IUTAM Symp. in Delft.

28. Niemunis A, Herle I. Hypoplastic model for cohesionless soils with elastic strain range. Mechanics of Cohesive-Frictional Materials 1997;2:279–299.

29. Niemunis A. On the estimation of the amplitude of shear strain from measurements in situ. Soil Dynamics and Earthquake Engineering 1995;14(1):1–3.

30. Niemunis A, Cudny M. On hyperplasticity for clays. Computers and Geotechnics 1998;23:221–236.

31. Shamoto Y, Sato M, Zhang JM. Simplified estimation of earthquake-induced settlements in saturated sand deposits. Soils and Foundations 1996;36(1):39–50.

32. Niemunis A, Wichtmann T, Triantafyllidis T. Compaction of freshly pluviated granulates under uniaxial and multiaxial cyclic loading. In: et al JV, editor, Geotechnical problems with man-made and man-influenced grounds. volume 1, 2003; pp. 855–860. XIIIth European Conference On Soil Mechanics and Geotechnical Engineering, Prague.

33. Wichtmann T, Niemunis A, Triantafyllidis T. Strain accumulation in sand due to cyclic loading: drained triaxial tests. Soil Dynamics and Earthquake Engineering 2005; Accepted for publication.

34. Triantafyllidis T, Wichtmann T, Niemunis A. On the determination of cyclic strain history. In: Triantafyllidis T, editor, Cyclic Behaviour of Soils and Liquefaction Phenomena. Balkema, 2004; pp. 321–334. International Conference in Bochum, 31 March - 02 April 2004.

35. Roscoe KH, Burland JB. On the generalized stress-strain behaviour of wet clays. In: Heyman J, Leckie FA, editors, Engineering plasticity. Cambridge University Press, 1968; pp. 535–609.

36. Ko H, Scott R. Deformation of sand in hydrostatic compression. Journal of Soil Mechanics and Foundations Division ASCE 1967;93(SM3):137–156.

37. Nicholson PG, Seed RB, Anwar HA. Elimination of membrane compliance in undrained triaxial testing. 1. measurement and evaluation. Canadian Geotechnical Journal 1993; 30:727–738.

38. Coop MR. On the mechanics of reconstituted and natural sands. In: Di Benedetto H, Doanh T, Geoffroy H, C S, editors, Deformation characteristics of geomaterials. Recent investigations and prospects. Balkema, 2005; pp. 29–58.

39. Ishihara K. Liquefaction and flow failure during earthquakes. Géotechnique 1993;43(3):351–415.

40. Miner M. Cumulative damage in fatigue. Transactions of the American Society of Mechanical Engineering 1945; 67:A159–A164.

41. Chopi C, Arduino P. Behavioral characteristics of gravelly soils under general cyclic loading conditions. In: Triantafyllidis T, editor, Cyclic Behaviour of Soils and Liquefaction Phenomena. Balkema, 2004; pp. 115–122. International Conference in Bochum, 31 March - 02 April 2004.

42. Hibbitt, Karlsson & Sorensen Inc. Abaqus 5.8 User's Manual Volume III, 1998.

43. Niemunis A. Akkumulation der Verformung infolge zyklischer Belastung des Bodens - numerische Strategien. In: Th Triantafyllidis, editor, Boden unter fast zyklischer Belastung: Erfahrungen und Forschungsergebnisse. Lehrstuhl für Grundbau und Bodenmechanik der Ruhr-Universität Bochum, volume 32, 2000; pp. 1–20.

44. Hammami M. Numerische Fehler bei der expliziten FE-Berechnung der Verdichtbarkeit von Sand infolge zyklischer Belastung, 2003. Master thesis.

45. Hughes TJR. The finite element method. Linear static and dynamic FE analysis. Dover Publications, 2000.

46. Helm J, Laue J, Triantafydillis T. Untersuchungen an der RUB zur Verformungsentwicklung von Böden unter zyklischen Beanspruchungen. In: Triantafyllidis T, editor, Böden unter fast zyklischer Belastung: Erfahrungen und Forschungsergebnisse. Lehrstuhl für Grundbau und Bodenmechanik, Ruhr-Universität Bochum, 2000; pp. 109–133.

47. Herle I. Hypoplastizität und Granulometrie einfacher Korngerüste. Ph.D. thesis, Institut für Boden- und Felsmechanik der Universität Karlsruhe, 1997. Nr. 142.